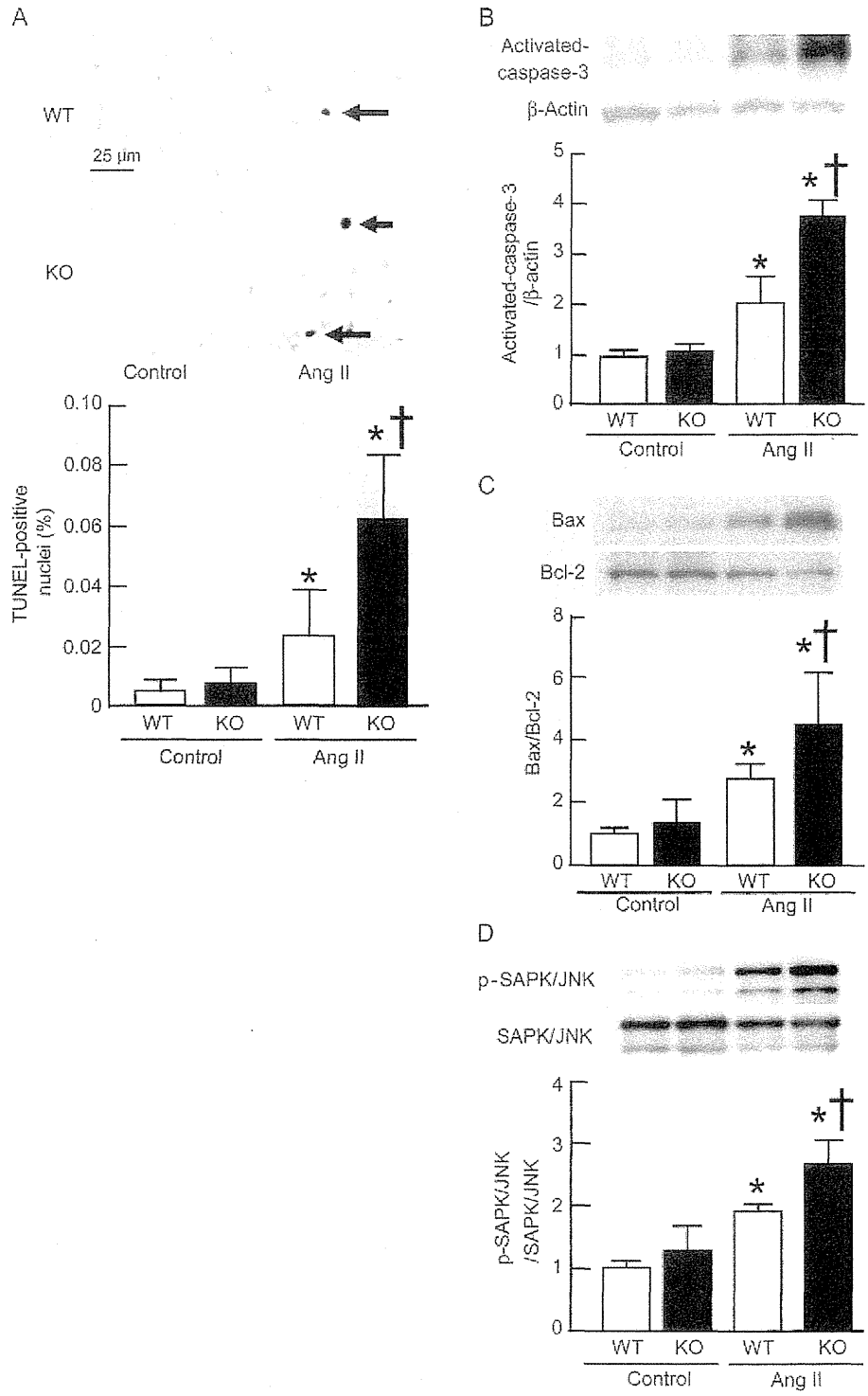

Figure 4 Apoptosis and apoptotic signalling pathways in WT and SMP30-KO mice after Ang II infusion. (*A*) Upper panels show representative images of TUNEL staining of left ventricular tissue sections. Lower bar graph shows the per cent of TUNEL-positive nuclei. (*B*) Activation of caspase-3 was examined by western blotting with anti-activated-caspase-3 antibody using myocardial samples. Expression levels of activated-caspase-3 were normalized by β-actin. (*C*) Expressions of Bax and Bcl-2 were analysed by western blotting. The Bax to Bcl-2 ratio was calculated and presented in the bar graph. (*D*) Phosphorylation activity of SAPK/JNK. Expressions of phosphorylated and total SAPK/JNK were analysed by western blotting. Relative expression levels of phosphorylated SAPK/jNK (P-SAPK/JNK) were expressed in relation to those of SAPK/JNK. Results are mean ± SD from 6 to 10 mice in each group. *$P < 0.01$ vs. control in the same strain mice; †$P < 0.01$ vs. Ang II-infused WT mice.

been investigated. In this study, we demonstrated the first evidence that deficiency of SMP30 exacerbates Ang II-induced cardiac hypertrophy, dysfunction, and adverse remodelling. Our results revealed that SMP30 has a cardio-protective role with anti-oxidative and anti-apoptotic effects in response to Ang II.

It has been well known that Ang II plays an important role in the development of pathological cardiac hypertrophy, remodelling, and subsequent heart failure.[33] Subcutaneous chronic infusion of Ang II induces cardiac hypertrophy and fibrosis with hypertension.[18,34] Ang II also stimulates NADPH oxidase to produce ROS,[35] and consequent myocardial oxidative stress is associated with the development of left ventricular remodelling and heart failure.[36] Furthermore, it has been considered that apoptosis plays an adverse role in cardiac remodelling and contributes to progressive myocardial dysfunction[37] and that Ang II exaggerates apoptotic responses in cardiomyocytes.[38] Interestingly, we observed that deficiency of SMP30 exacerbates Ang II-induced cardiac hypertrophy and fibrosis in SMP30-KO mice (*Table 1*, *Figure 2*, and Supplementary material online, *Figure S1*). Moreover, we found that Ang II-infused SMP30-KO mice showed left ventricular dilatation and depressed systolic function in addition to more severely impaired diastolic function compared with Ang II-infused WT mice, suggesting that the absence of SMP30 caused more progressive cardiac dysfunction and remodelling (*Table 1* and Supplementary material online, *Table S1* and *Figure S2*). These remarkable changes were independent of Ang II-induced hypertension because increased systemic blood pressure of SMP30-KO mice was similar to that of WT mice (*Table 1*). SMP30-KO mice had much more elevated NADPH oxidase-generated ROS by Ang II stimulation (*Figure 3*). In addition, SMP30-KO mice were more susceptible to Ang II-induced apoptosis associated with activation of caspase-3, increase in Bax, decrease in Bcl-2, and phosphorylation of SAPK/JNK (*Figure 4*). Although we were unable to show the direct observation of TUNEL-positive cardiomyocyte nuclei, apoptosis of non-cardiomyocytes plays an important role in Ang II-induced cardiac remodelling and dysfunction as previously reported.[39] These data indicate that SMP30 has a protective role against Ang II-associated cardiac hypertrophy, dysfunction, and remodelling by inhibiting oxidative stress and apoptosis.

SMP30 has been proposed as an important ageing marker, and the lack of SMP30 causes various dysfunctions of organs during ageing process.[11,13–15] Concerning the vitamin C biosynthesis pathway, similar to humans, SMP30-KO mice cannot synthesize vitamin C and SMP30-KO mice may mimic the human physiology closer than other rodents.[40] The potent anti-ageing and anti-oxidative actions of a low-calorie diet effectively suppressed the age-related down-regulation of SMP30, indicating that SMP30 expression was influenced by oxidative stress.[41] These previous reports suggest that SMP30 expression accounts for the age-associated deterioration of cellular function and the enhanced susceptibility to harmful stimuli in aged tissues. On the other hand, very few reports demonstrated cellular senescence of cardiomyocytes *in vivo*.[42,43] We demonstrated that Ang II could increase senescent cells detected by SA β-gal activity *in vivo*. Importantly, Ang II-induced cellular senescence was accompanied with markedly elevated p21 gene expression. SMP30-KO mice showed significantly increased SA β-gal-positive cells with elevated expression of p21 gene by Ang II stimulation, indicating that SMP30 inhibits premature cellular senescence through the signalling pathway of p21 in response to Ang II (*Figure 5*).

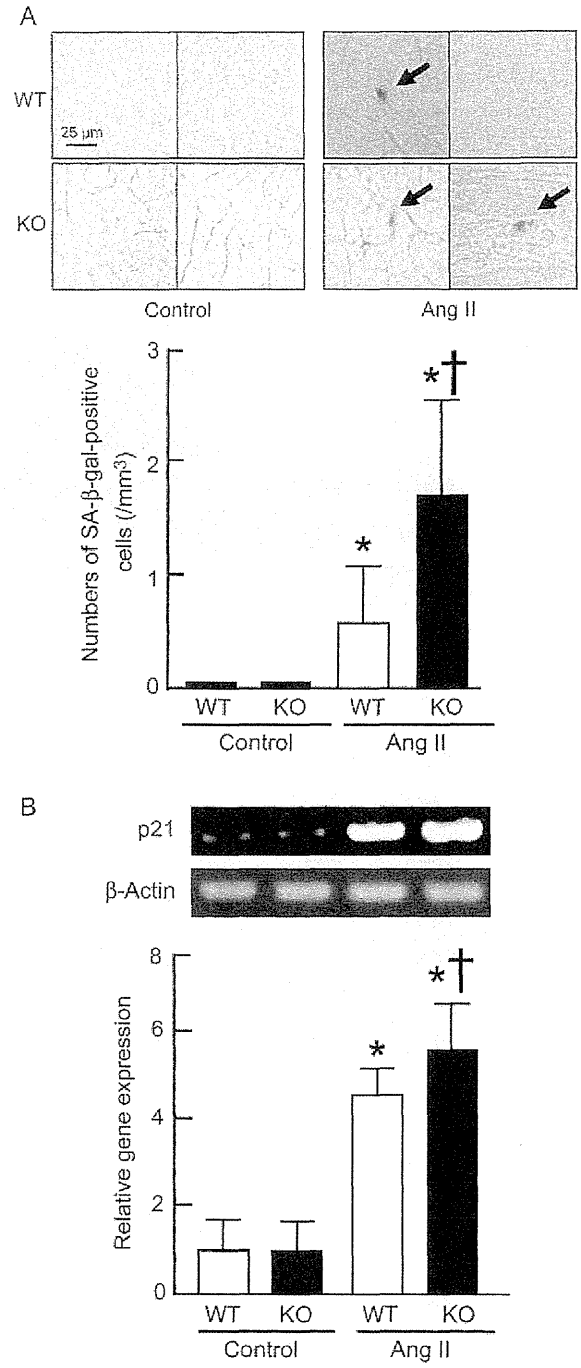

Figure 5 Senescence markers in hearts of WT and SMP30-KO mice after Ang II infusion. (*A*) Senescent cells were detected by SA β-gal staining of left ventricular tissue sections, and the numbers of SA β-gal-positive cells were counted. (*B*) The mRNA expression levels of p21 gene were analysed by RT–PCR. Expression levels of p21 gene were normalized by β-actin. Results are mean ± SD from 6 to 8 mice in each group. $^{*}P < 0.01$ vs. control in the same strain mice; $^{\dagger}P < 0.01$ vs. Ang II-infused WT mice.

There were no differences between WT mice and SMP30-KO mice under basal conditions at 12- to 16-week-old, but we observed that 12-month-old SMP30-KO mice showed exaggerated left ventricular hypertrophy, diastolic dysfunction, and myocardial fibrosis compared with 12-month-old WT mice (Supplementary material online, *Table S2*). One central role of SMP30 in the heart is considered to be the suppressive effect of ROS generation by inhibiting NADPH oxidase activation, as demonstrated in the present study (*Figure 3*). The suppressive role of SMP30 in oxidative stress contributes to the reduction of senescent marker expressions, suggesting that SMP30 prevents myocardial dysfunction from various stresses such as Ang II stimulation and ageing (Supplementary material online, *Figure S3*). Since detailed mechanisms have not been fully clarified, we should evaluate the cellular compartment specific effects of SMP30 in the future study.

5. Conclusions

In summary, deficiency of SMP30 adversely modifies Ang II-induced cardiac hypertrophy and remodelling through increase in oxidative stress and progression of apoptosis. These data provide that SMP30 has a protective role in cardiac remodelling and up-regulation of SMP30 could be a therapeutic target for treatment of heart failure.

Supplementary material

Supplementary material is available at *Cardiovascular Research* online.

Acknowledgements

We thank Ms. Emiko Kaneda for the excellent technical assistance.

Conflict of interest: none declared.

Funding

This study was supported in part by a grant-in-aid for Scientific Research (No. 24591100, Y.T.) from the Japan Society for the Promotion of Science.

References

1. Lakatta EG, Levy D. Arterial and cardiac aging: major shareholders in cardiovascular disease enterprises: part II: the aging heart in health: links to heart disease. *Circulation* 2003;**107**:346–354.
2. Lakatta EG. Arterial and cardiac aging: major shareholders in cardiovascular disease enterprises: part III: cellular and molecular clues to heart and arterial aging. *Circulation* 2003;**107**:490–497.
3. Wang M, Zhang J, Walker SJ, Dworakowski R, Lakatta EG, Shah AM. Involvement of NADPH oxidase in age-associated cardiac remodeling. *J Mol Cell Cardiol* 2010;**48**:765–772.
4. Fujita T, Uchida K, Maruyama N. Purification of senescence marker protein-30 (SMP30) and its androgen-independent decrease with age in the rat liver. *Biochim Biophys Acta* 1992;**1116**:122–128.
5. Fujita T, Mandel JL, Shirasawa T, Hino O, Shirai T, Maruyama N. Isolation of cDNA clone encoding human homologue of senescence marker protein-30 (SMP30) and its location on the X chromosome. *Biochim Biophys Acta* 1995;**1263**:249–252.
6. Arun P, Aleti V, Parikh K, Manne V, Chilukuri N. Senescence marker protein 30 (SMP30) expression in eukaryotic cells: existence of multiple species and membrane localization. *PLoS ONE* 2011;**6**:e16545.
7. Shimokawa N, Yamaguchi M. Molecular cloning and sequencing of the cDNA coding for a calcium-binding protein regucalcin from rat liver. *FEBS Lett* 1993;**327**:251–255.
8. Son TG, Kim SJ, Kim K, Kim MS, Chung HY, Lee J. Cytoprotective roles of senescence marker protein 30 against intracellular calcium elevation and oxidative stress. *Arch Pharm Res* 2008;**31**:872–877.
9. Little JS, Broomfield CA, Fox-Talbot MK, Boucher LJ, MacIver B, Lenz DE. Partial characterization of an enzyme that hydrolyzes sarin, soman, tabun, and diisopropyl phosphorofluoridate (DFP). *Biochem Pharmacol* 1989;**38**:23–29.
10. Kondo Y, Inai Y, Sato Y, Handa S, Kubo S, Shimokado K *et al.* Senescence marker protein 30 functions as gluconolactonase in L-ascorbic acid biosynthesis, and its knockout mice are prone to scurvy. *Proc Natl Acad Sci USA* 2006;**103**:5723–5728.
11. Ishigami A, Fujita T, Handa S, Shirasawa T, Koseki H, Kitamura T *et al.* Senescence marker protein-30 knockout mouse liver is highly susceptible to tumor necrosis factor-alpha- and Fas-mediated apoptosis. *Am J Pathol* 2002;**161**:1273–1281.
12. Ishigami A, Kondo Y, Nanba R, Ohsawa T, Handa S, Kubo S *et al.* SMP30 deficiency in mice causes an accumulation of neutral lipids and phospholipids in the liver and shortens the life span. *Biochem Biophys Res Commun* 2004;**315**:575–580.
13. Son TG, Zou Y, Jung KJ, Yu BP, Ishigami A, Maruyama N *et al.* SMP30 deficiency causes increased oxidative stress in brain. *Mech Ageing Dev* 2006;**127**:451–457.
14. Sato T, Seyama K, Sato Y, Mori H, Souma S, Akiyoshi T *et al.* Senescence marker protein-30 protects mice lungs from oxidative stress, aging, and smoking. *Am J Respir Crit Care Med* 2006;**174**:530–537.
15. Yamura W, Imasawa T, Suganuma S, Isnigami A, Handa S, Kubo S *et al.* Accelerated tubular cell senescence in SMP30 knockout mice. *Histol Histopathol* 2006;**21**:1151–1156.
16. Hasegawa G, Yamasaki M, Kadono M, Tanaka M, Asano M, Senmaru T *et al.* Senescence marker protein-30/gluconolactonase deletion worsens glucose tolerance through impairment of acute insulin secretion. *Endocrinology* 2010;**151**:529–536.
17. Xue B, Pamidimukkala J, Lubahn DB, Hay M. Estrogen receptor-alpha mediates estrogen protection from angiotensin II-induced hypertension in conscious female mice. *Am J Physiol Heart Circ Physiol* 2007;**292**:H1770–H1776.
18. Kobayashi A, Ishikawa K, Matsumoto H, Kimura S, Kamiyama Y, Maruyama Y. Synergetic antioxidant and vasodilatory action of carbon monoxide in angiotensin II-induced cardiac hypertrophy. *Hypertension* 2007;**50**:1040–1048.
19. Tsao CS, Leung PY, Young M. Effect of dietary ascorbic acid intake on tissue vitamin C in mice. *J Nutr* 1987;**117**:291–297.
20. Carlson SH, Wyss JM. Long-term telemetric recording of arterial pressure and heart rate in mice fed basal and high NaCl diets. *Hypertension* 2000;**35**:E1–E5.
21. Du J, Liu J, Feng HZ, Hossain MM, Gobara N, Zhang C *et al.* Impaired relaxation is the main manifestation in transgenic mice expressing a restrictive cardiomyopathy mutation, R193H, in cardiac TnI. *Am J Physiol Heart Circ Physiol* 2008;**294**:H2604–H2613.
22. Wilson RM, De Silva DS, Sato K, Izumiya Y, Sam F. Effects of fixed-dose isosorbide dinitrate/hydralazine on diastolic function and exercise capacity in hypertension-induced diastolic heart failure. *Hypertension* 2009;**54**:583–590.
23. Kitahara T, Takeishi Y, Harada M, Niizeki T, Suzuki S, Sasaki T *et al.* High-mobility group box 1 restores cardiac function after myocardial infarction in transgenic mice. *Cardiovasc Res* 2008;**80**:40–46.
24. Arimoto T, Takeishi Y, Takahashi H, Shishido T, Niizeki T, Koyama Y *et al.* Cardiac-specific overexpression of diacylglycerol kinase zeta prevents Gq protein-coupled receptor agonist-induced cardiac hypertrophy in transgenic mice. *Circulation* 2006;**113**:60–66.
25. Takimoto E, Champion HC, Li M, Ren S, Rodriguez ER, Tavazzi B *et al.* Oxidant stress from nitric oxide synthase-3 uncoupling stimulates cardiac pathologic remodeling from chronic pressure load. *J Clin Invest* 2005;**115**:1221–1231.
26. Machii H, Saitoh S, Kaneshiro T, Takeishi Y. Aging impairs myocardium-induced dilation in coronary arterioles: role of hydrogen peroxide and angiotensin. *Mech Ageing Dev* 2010;**131**:710–717.
27. Matsushima S, Kinugawa S, Yokota T, Inoue N, Ohta Y, Hamaguchi S *et al.* Increased myocardial NAD(P)H oxidase-derived superoxide causes the exacerbation of postinfarct heart failure in type 2 diabetes. *Am J Physiol Heart Circ Physiol* 2009;**297**:H409–H416.
28. Nozaki N, Shishido T, Takeishi Y, Kubota I. Modulation of doxorubicin-induced cardiac dysfunction in toll-like receptor-2-knockout mice. *Circulation* 2004;**110**:2869–2874.
29. Dimri GP, Lee X, Basile G, Acosta M, Scott G, Roskelley C *et al.* A biomarker that identifies senescent human cells in culture and in aging skin *in vivo*. *Proc Natl Acad Sci USA* 1995;**92**:9363–9367.
30. Camelliti P, Borg TK, Kohl P. Structural and functional characterisation of cardiac fibroblasts. *Cardiovasc Res* 2005;**65**:40–51.
31. Yue TL, Wang C, Romanic AM, Kidy K, Keller P, DeWolf WE Jr *et al.* Staurosporine-induced apoptosis in cardiomyocytes: a potential role of caspase-3. *J Mol Cell Cardiol* 1998;**30**:495–507.
32. Aoki H, Kang PM, Hampe J, Yoshimura K, Noma T, Matsuzaki M *et al.* Direct activation of mitochondrial apoptosis machinery by c-Jun N-terminal kinase in adult cardiac myocytes. *J Biol Chem* 2002;**277**:10244–10250.
33. Weber KT, Brilla CG. Pathological hypertrophy and cardiac interstitium. Fibrosis and renin-angiotensin-aldosterone system. *Circulation* 1991;**83**:1849–1865.
34. Izumiya Y, Kim S, Izumi Y, Yoshida K, Yoshiyama M, Matsuzawa A *et al.* Apoptosis signal-regulating kinase 1 plays a pivotal role in angiotensin II-induced cardiac hypertrophy and remodeling. *Circ Res* 2003;**93**:874–883.
35. Mollnau H, Wendt M, Szocs K, Lassegue B, Schulz E, Oelze M *et al.* Effects of angiotensin II infusion on the expression and function of NAD(P)H oxidase and components of nitric oxide/cGMP signaling. *Circ Res* 2002;**90**:E58–E65.
36. Giordano FJ. Oxygen, oxidative stress, hypoxia, and heart failure. *J Clin Invest* 2005;**115**:500–508.
37. Olivetti G, Abbi R, Quaini F, Kajstura J, Cheng W, Nitahara JA *et al.* Apoptosis in the failing human heart. *N Engl J Med* 1997;**336**:1131–1141.

38. Ravassa S, Fortuno MA, Gonzalez A, Lopez B, Zalba G, Fortuno A *et al.* Mechanisms of increased susceptibility to angiotensin II-induced apoptosis in ventricular cardiomyocytes of spontaneously hypertensive rats. *Hypertension* 2000;**36**:1065–1071.
39. Park M, Sher YT, Gaussin V, Heyndrickx GR, Bartunek J, Resuello RR *et al.* Apoptosis predominates in nonmyocytes in heart failure. *Am J Physiol Heart Circ Physiol* 2009;**297**: H785–H791.
40. Yu R, Schellhorn HE. Recent applications of engineered animal antioxidant deficiency models in human nutrition and chronic disease. *J Nutr* 2013;**143**:1–11.
41. Jung KJ, Ishigami A, Maruyama N, Takahashi R, Goto S, Yu BP *et al.* Modulation of gene expression of SMP-30 by LPS and calorie restriction during aging process. *Exp Gerontol* 2004;**39**:1169–1177.
42. Inuzuka Y, Okuda J, Kawashima T, Kato T, Niizuma S, Tamaki Y *et al.* Suppression of phosphoinositide 3-kinase prevents cardiac aging in mice. *Circulation* 2009;**120**:1695–1703.
43. Maejima Y, Adachi S, Ito H, Hirao K, Isobe M. Induction of premature senescence in cardiomyocytes by doxorubicin as a novel mechanism of myocardial damage. *Aging Cell* 2008;**7**:125–136.

Human Mutation

OFFICIAL JOURNAL

HGVS

HUMAN GENOME VARIATION SOCIETY

www.hgvs.org

Dilated Cardiomyopathy-Associated *BAG3* Mutations Impair Z-Disc Assembly and Enhance Sensitivity to Apoptosis in Cardiomyocytes

Takuro Arimura,[1] Taisuke Ishikawa,[1] Shinichi Nunoda,[2] Sachio Kawai,[3] and Akinori Kimura[1,4]*

[1]*Department of Molecular Pathogenesis, Medical Research Institute, Tokyo Medical and Dental University, Tokyo, Japan;* [2]*Department of Medicine, Tokyo Women's Medical University Medical Center East, Tokyo, Japan;* [3]*Department of Sports Medicine, Juntendo University Graduate School of Health and Sports Science, Tokyo, Japan;* [4]*Laboratory of Genome Diversity, School of Biomedical Science, Tokyo Medical and Dental University, Tokyo, Japan*

Communicated by Mark H. Paalman

Received 4 May 2011; accepted revised manuscript 24 August 2011.

Published online 6 September 2011 in Wiley Online Library (www.wiley.com/humanmutation).DOI: 10.1002/humu.21603

ABSTRACT: Dilated cardiomyopathy (DCM) is characterized by dilation of left ventricular cavity with systolic dysfunction. Clinical symptom of DCM is heart failure, often associated with cardiac sudden death. About 20–35% of DCM patients have apparent family histories and it has been revealed that mutations in genes for sarcomere proteins cause DCM. However, the disease-causing mutations can be found only in about 17% of Japanese patients with familial DCM. Bcl-2-associated athanogene 3 (BAG3) is a co-chaperone protein with antiapoptotic function, which localizes at Z-disc in the striated muscles. Recently, *BAG3* gene mutations in DCM patients were reported, but the functional abnormalities caused by the mutations are not fully unraveled. In this study, we analyzed 72 Japanese familial DCM patients for mutations in *BAG3* and found two mutations, p.Arg218Trp and p.Leu462Pro, in two cases of adult-onset DCM without skeletal myopathy, which were absent from 400 control subjects. Functional studies at the cellular level revealed that the DCM-associated *BAG3* mutations impaired the Z-disc assembly and increased the sensitivities to stress-induced apoptosis. These observations suggested that *BAG3* mutations present in 2.8% of Japanese familial DCM patients caused DCM possibly by interfering with Z-disc assembly and inducing apoptotic cell death under the metabolic stress.

Hum Mutat 32:1481–1491, 2011.

KEY WORDS: dilated cardiomyopathy; DCM; *BAG3*

Introduction

Dilated cardiomyopathy (DCM) is a primary heart muscle disorder caused by functional abnormalities in the cardiomyocytes, which is characterized by ventricular chamber dilation and diminished cardiac contractility. DCM is a major cause of chronic heart failure and the most common indication for cardiac transplantation [Maron et al., 2006]. Various etiologies including gene mutations, viral infections, toxins such as alcohol, mitochondrial abnormalities, and metabolic disorders cause DCM [Maron et al., 2006]. Because 20 to 35% of DCM patients have family histories mostly consistent with autosomal dominant inheritance, linkage studies in multiplex families and/or candidate gene approaches have been taken to identify the disease genes and it has been revealed that DCM can be caused by various genetic abnormalities [Kimura, 2010]. The majority of genetic causes are heterozygous mutations in genes for sarcomere proteins including contractile elements, sarcolemma elements, Z-disc elements, and Z-I region components, which play key roles in the generation and/or transmission of contractile force. On the other hand, it has recently been demonstrated by extensive whole-genome analyses that sequence variations in the gene for Bcl-2-associated athanogene 3 (*BAG3*; MIM# 603883) were associated with DCM (CMD1HH; MIM# 613881) [Norton et al., 2011; Villard et al., 2011], although molecular mechanisms of DCM caused by the *BAG3* mutations are not fully unraveled.

BAG3 is a member of antiapoptotic BAG protein family. BAG3 protein binds heat shock protein 70 (Hsp70; MIM# 140550) within the C-terminal BAG domain, which is an evolutionary conserved domain among the BAG family, and serves as a co-chaperone factor controlling the chaperone activity of Hsp70 [Takayama et al., 1999]. It was reported that *BAG3* prominently expressed in the striated muscle and localized at the Z-discs [Homma et al., 2006]. In addition, *Bag3* knockout mice displayed degeneration of muscle fibers with apoptotic nuclei in the striated muscles, resulting in a severe form of skeletal myopathy and cardiomyopathy, which lead to a hypothesis that BAG3 protein might play a role as a Z-disc signaling molecule [Homma et al., 2006]. In accordance with the hypothesis, apart from the association with DCM described above [Norton et al., 2011; Villard et al., 2011], a heterozygous Pro209Leu mutation was found in patients with myofibrillar myopathy (MFM) accompanied by cardiomyopathy (MFM6; MIM# 612954) [Lee et al., 2011; Odgerel et al., 2010; Selcen et al., 2009]. Moreover, it was demonstrated that knockdown of *bag3* in a zebrafish model developed heart failure resembling to human DCM [Norton et al., 2011].

*Correspondence to: Akinori Kimura, Department of Molecular Pathogenesis, Medical Research Institute, Tokyo Medical and Dental University, 1-5-45 Bunkyo-Ku, Tokyo 113-8510, Japan. E-mail: akitis@mri.tmd.ac.jp

Contract grant sponsors: Ministry of Education, Culture, Sports, Science and technology, Japan; Ministry of Health, Labor and Welfare, Japan; Japan Society for the Promotion of Science: Basic Scientific Cooperation Program between Japan and Korea; Association Française contre les Myopathies (AFM); Institute of Life Science; Tokyo Medical and Dental University.

We report here two heterozygous *BAG3* gene mutations, identified in Japanese patients with familial DCM, which cause abnormal Z-disc assembly and increase the sensitivity to apoptosis in cultured cardiomyocytes. This is the first report demonstrating that the stress-induced apoptotic cell death accompanied by abnormal sarcomerogenesis is associated with DCM.

Materials and Methods

Subjects

A total of 72 genetically unrelated Japanese patients with DCM were included in this study. Each patient had an apparent family history (at least one patient among the first-degree family relatives). The patients were diagnosed based on medical history, physical examination, 12-lead electrocardiogram, echocardiography, and other special tests if necessary. The diagnostic criteria for DCM were described previously [Hayashi et al., 2004] and the patients who manifested with apparent skeletal muscle involvement were excluded from the study. The patients had been analyzed for mutations in 22 known cardiomyopathy-associated genes including genes for titin/connectin (*TTN*), desmin (*DES*), αB-crystallin (*CRYAB*), ZASP/Cypher (*LDB3*), and four-and-half LIM protein 2 (*FHL2*) [Kimura, 2010], and no mutation was found in any of them. Four hundred Japanese healthy individuals served as controls. Blood samples were obtained from each subject after given informed consent. The protocol for research was approved by the Ethics Review Committee of Medical Research Institute, Tokyo Medical and Dental University, Tokyo, Japan.

Mutational Analysis

Genomic deoxyribonucleic acids (DNAs) extracted from peripheral blood of subjects were used to amplify protein-coding exons of *BAG3* (GenBank Accession No. NM_004281.3) by polymerase chain reaction (PCR) in exon-by-exon manner using primer pairs; 5′-CGAGGAGGCTATTTCCAGAC-3′ and 5′-TGCCGTCGAGGTGGCGCCACCGACC-3′ for exon 1, 5′-AGTGTTTCCTCTGCCAGGAG-3′ and 5′-TGGGAAGCACAGCGGCTTGCTC-3′ for exon 2, 5′-CAAGCCAGGGGAGTCATTTG-3′ and 5′-GACATACCACCATAACCAGTC-3′ for exon 3, 5′-CAATTTCTGTGACTTTCAGTCAG-3′ and 5′-GTCAGTCTTCTTGCCTTCAAAG-3′ for the 5′-side half of exon 4, and 5′-ATCCAGGAGTGCTGAAAGTG-3′ and 5′-AAGTCTCTGAAATGCATGCAAC-3′ for the 3′-side half of exon 4. The PCR condition was composed of a denaturing step of 95°C for 2 min, 30 cycles of 95°C for 30 sec, 56°C for 30 sec, and 72°C for 30 sec, followed by an additional extension step of 72°C for 2 min. The PCR products were analyzed by direct sequencing on both strands using Big Dye Terminator chemistry (version 3.1) and ABI3100 DNA Analyzer (Applied Biosystems, CA).

Amino Acid Sequence Comparison of BAG3 from Various Species

Amino acid sequences of human BAG3 protein predicted from NM_004281.3 were aligned with those of rhesus monkey (XM_001104106), cattle (NM_001082471), rat (NM_001011936), mouse (NM_013863), chicken (XM_001233434), xenopus (BC043807), and zebrafish (BC078249).

Indirect Immunofluorescence Microscopy

Complementary DNA (cDNA) of human *BAG3* were obtained by reverse transcriptase PCR from total messenger ribonucleic acid of adult heart. A wild-type (WT) full-length *BAG3* cDNA fragment spanned from bp307 to bp2034 of NM_004281.3 (corresponding to aa1-aa576). Five equivalent mutant cDNA fragments carrying a C to T (MFM-associated Pro209Leu mutation) [Selcen et al., 2009], a C to T (DCM-associated Arg218Trp mutation), a C to T (nondisease-associated Arg258Trp polymorphism), or a T to C (DCM-associated Leu462Pro mutation) substitution were obtained by the primer-directed mutagenesis method. The cDNA fragments of *BAG3* were cloned into pEGFP-C1 vector (Clontech, CA) and they were sequenced to ensure that no errors were introduced.

All care and treatment of animals were in accordance with the guidelines for the Care and Use of Laboratory Animals published by the National Institute of Health (NIH Publication 85-23, revised 1985) and subjected to prior approval by the local animal protection authority. Neonatal rat cardiomyocytes (NRCs) from one-day-old Sprague-Dawley rats were prepared as described previously [Arimura et al., 2009]. NRCs (1×10^4 cells) were plated onto the Collagen Type I Cellware 8-Well Culture Slide (BD Biosciences, MA) in low-glucose DMEM supplemented with 0.01 mg/ml insulin (Sigma-Aldrich, MO), 10% fetal bovine serum (FBS), and 1% penicillin/streptomycin at 37°C with 5% CO_2 for 24 hr. Each pEGFP-based construct (0.3 μg) was transfected into the cells with 0.6 μl of TransFectin Lipid Reagent (Bio-Rad, CA), according to the manufacturer's instructions. Forty-eight hours after the transfection, the NRCs were washed with PBS and fixed for 15 min in 100% ethanol at −20°C. Transfected cells were incubated in blocking solution and stained by primary mouse anti-α-actinin (1:800, Sigma-Aldrich) or anti-desmin (1:200, Dako, Glostrup, Denmark), followed by secondary Alexa fluor 568 goat anti-mouse IgG_1 (1:500, Molecular Probes, OR).

C2C12 cells (8×10^3 cells), a mouse myoblast cell line, were plated onto the gelatin-coated Lab-Tek 2 well Chamber Slide (Nalgen Nunc International, NY) in DMEM supplemented with 20% FBS and 1% penicillin/streptomycin at 37°C with 5% CO_2 for 24 hr. The cells were transfected with each pEGFP-based construct (2 μg) in 4 μl of Turbofect in vitro Transfection Reagent (Fermentas Inc., ML) according to the manufacturer's instructions. Forty-eight hours after the transfection, the cells were cultured in differentiation medium (DMEM with 2% horse serum, 0.01 mg/ml insulin, and 1% penicillin/streptomycin) for 5 days. Differentiated myotubes were washed with PBS, fixed for 15 min in 100% ethanol at −20°C, incubated in blocking solution, and stained by primary mouse anti-MF20 (1:50, DSHB in University of Iowa, IA) monoclonal antibody (Ab), followed by secondary Alexa fluor 568 goat anti-mouse IgG (1:500, Molecular Probes).

All cells were mounted on a cover-glass using Mowiol 4-88 Reagent (Calbiochem, Darmstadt, Germany) with 4′6-diamidino-2-phenylindole (DAPI, Sigma-Aldrich), and images from at least 200 transfected cells were analyzed by using the LSM510 laser-scanning microscope (Carl Zeiss Microscopy, Jena, Germany).

Apoptosis Assay

For the apoptosis assay, 24 hr after the transfection with *BAG3* constructs, the NRCs were cultured under serum-deprived (FBS-free medium) condition for additional 24 hr, washed with PBS, fixed for 1 hr in 4% paraformaldehyde/PBS at room temperature, and permeabilized for 2 min in 0.1% Triton X-100/0.1%

sodium citrate on ice. Apoptosis was evaluated with the terminal deoxynucleotidyltransferase-mediated dUTP nick end-labeling (TUNEL) assay using in situ Cell Death Detection Kit, TMR red (Roche Diagnostics, Mannheim, Germany) according to the manufacturer's instructions.

Quantitative analysis of apoptosis was performed with the Cell Death Detection ELISA^{PLUS} kit (Roche Diagnostics) according to the manufacturer's instructions. H9c2 cells, a cell line derived from rat embryonic ventricular myocardial cells, were cultured in DMEM supplemented with 10% FBS and 1% penicillin/streptomycin at 37°C with 5% CO_2. The *BAG3* constructs were transfected into H9c2 cells using the TransFectin Lipid Reagent (Bio-Rad) according to the manufacturer's instructions, and transfectants were selected using Geneticin (Life Technologies Japan Ltd., Tokyo, Japan). After establishment of the stable H9c2 transfectants, 4×10^3 cells in each line were plated onto collagen type I-coated 96-well plates. Doxorubicin (1 μM; Sigma-Aldrich) was added to culture media and the cells were cultured for various intervals (24, 48, and 72 hr). Cells were lysed with 0.2 ml of the lysis buffer provided in the kit at room temperature for 30 min. Quantities of histone-associated DNA fragments (mono- and oligonucleosomes) were determined by an absorbance at 405 nm and a reference at 490 nm. Numerical data were arbitrarily expressed as means ± SEM. Statistical differences were analyzed using two-way analysis of variance and then evaluated using a Turkey adjustment for post hoc multiple comparison. A *P*-value of less than 0.05 was considered to be statistically significant.

Results

Identification of BAG3 Mutations in DCM

We searched for *BAG3* variations in 72 proband patients with familial DCM and eight distinct variations were identified (Fig. 1A). Among them, two synonymous substitutions, Pro334Pro (c.1002T>G in exon 4, rs3858339) and Val432Val (c.1296A>G in exon 4, rs196295), and three nonsynonymous variations, Arg258Trp (c.772C>T in exon 3, rs117671123), Asp300Asn (c.898G>A in exon 3, rs78439745), and Pro407Leu (c.1220C>T in exon 4, rs3858340), were known polymorphisms registered in the dbSNP database (http://www.ncbi.nlm.nih.gov/projects/SNP/). In addition, a nonsynonymous variation, Glu553Asp (c.1659A>T in exon 4) found in one patient, was considered to be a polymorphism, because it was found in heterozygous state in nine of the 400 control subjects, that is allele frequency was 0.011 in Japanese patients.

On the other hand, two missense mutations, Arg218Trp (c.652C>T in exon 3) and Leu462Pro (c.1385T>C in exon 4), identified in heterozygous state in two DCM patients (designated II-1 in Fig. 1B and C, respectively) were not observed in the 400 control subjects. A family study suggested a co-segregation of the Leu462Pro mutation with DCM, because the mutation was present in a possibly affected sister, but not present in her father and brother who did not suffer from DCM (Fig. 1C). Most of the *BAG3* sequence variations including polymorphisms were found at the residues that were evolutionary conserved from various species except for zebrafish (Fig. 1D).

Clinical parameters of the patients with *BAG3* mutations are shown in Table 1. The proband patients carrying Arg218Trp or Leu462Pro mutation developed DCM at age 73 or 34, respectively, suggesting that the mutations was associated with DCM of adult onset. It should be noted that a sister of patient carrying the Leu462Pro mutation did not manifest with overt DCM at age 27, but she showed a slight systolic dysfunction of heart. Electrocardiogram findings of the affected individuals demonstrated no primary conduction defect. Serum creatine kinase (CK) level was not increased in both cases with the Leu462Pro mutation. They did not show apparent sign of skeletal myopathy or neuropathy.

Abnormal Assembly of Z-Discs Caused by the DCM-Associated BAG3 Mutations in NRCs

To investigate a possible functional consequence of the *BAG3* mutations, we analyzed cellular distribution of BAG3 proteins by using green fluorescence protein (GFP) chimeras of *BAG3* transfected into NRCs. For this purpose, we constructed GFP-tagged BAG3 of WT and DCM-associated mutations, Arg218Trp and Leu462Pro. We also tested an MFM-associated mutation, Pro209Leu [Lee et al., 2011; Odgerel et al., 2010; Selcen et al., 2009], and a nondisease-related missense variant, Arg258Trp (Fig. 1A), which was found in one patient and 11 controls in this study. Control NRCs transfected with GFP-alone construct showed diffuse localization of GFP signals (data not shown). Western blot analyses showed that the expression of each GFP–BAG3 construct was similar at the protein level in the transfected cells, suggesting that the mutation did not affect the expression of GFP–BAG3 (data not shown). In the mature myofibrils where Z-discs were well organized, GFP-BAG3-WT was assembled in the striated pattern and co-localized with α-actinin and desmin, markers for the Z-disc (Figs. 2A–C and 3A–C, respectively). It was found that most (~90%) of NRCs did not show nuclear localization of GFP-BAG3-WT (Figs. 2A–C and 3A–C). GFP-BAG3-Pro209Leu and GFP-BAG3-Arg258Trp also showed striated pattern co-localized with α-actinin and desmin at the Z-discs and did not show the nuclear localization (Figs. 2D–F and 3D–F, and Figs. 2J–L and 3J–L, respectively). In clear contrast, striated distribution was not found for both GFP-BAG3-Arg218Trp (Figs. 2G–I and 3G–I) and GFP-BAG3-Leu462Pro (Figs. 2M–O and 3M–O) in about 90% of transfected NRCs. Of note was that the Z-disc assembly represented by localization of α-actinin and desmin was impaired in the NRCs transfected with GFP-BAG3-Arg218Trp or GFP-BAG3-Leu462Pro (Figs. 2H and 3H, or Figs. 2N and 3N, respectively). Quite interestingly, these mutant proteins displayed localization within the nuclei in approximately 80% of the transfected NRCs (Figs. 2G and 3G, or Figs. 2M and 3M, respectively). These data suggested that the DCM-associated mutations disturbed the assembly and integrity of Z-discs, along with the nuclear localization of BAG3 protein, while such abnormalities were not observed with the MFM-associated mutations.

Myotube Formation was Affected by the MFM-Associated BAG3 Mutation but Not by the DCM-Associated BAG3 Mutations in C2C12 Cells

The DCM patients carrying *BAG3* mutations in this study did not manifest with apparent skeletal muscle involvement, but some other *BAG3* mutations were reported in patients with MFM. There is a possibility that the DCM-associated mutations might affect the function of BAG3 protein in striated muscles differently from the MFM-associated mutation. To investigate whether the *BAG3* mutations would affect the skeletal muscle differentiation from myoblasts to myotubes, C2C12 myoblast cells were transfected with BAG3 constructs and differentiated into multinucleated myotubes by low-serum culture condition. After 5 days of differentiation, myosin heavy chain positive (recognized by MF20 Ab) myotubes could often be observed in this condition. Control cells transfected with GFP-alone construct (data not shown) and the

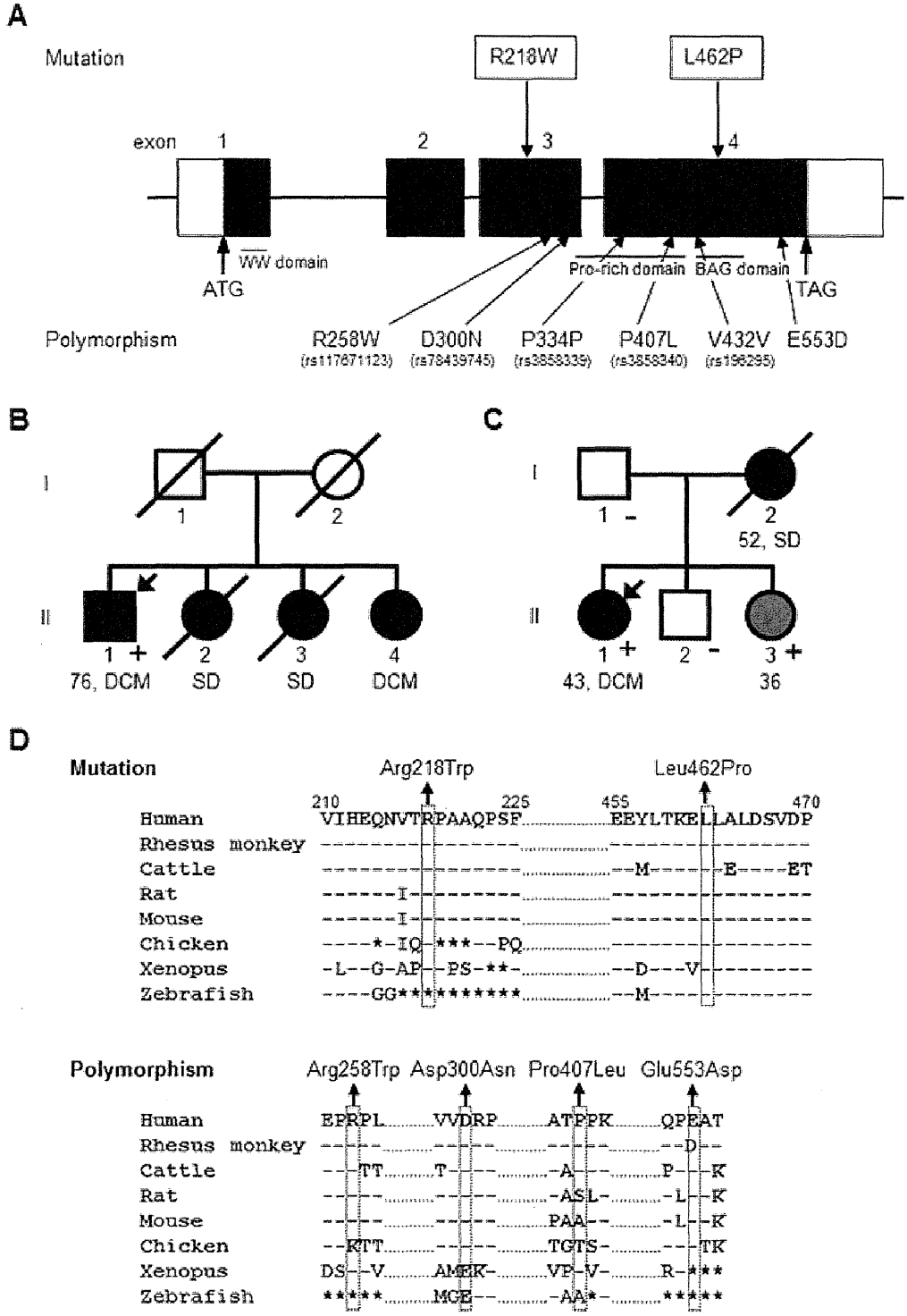

Figure 1. Mutational analysis of *BAG3* in dilated cardiomyopathy. A: Sequence variations found in this study are listed. Single-letter code is used to indicate the amino acid residue. DCM-associated mutations and polymorphisms are indicated above and below the schematic representation of *BAG3* gene, respectively. Known polymorphisms are indicated with reference single nucleotide polymorphism (rs) number in the parentheses. Solid boxes represent coding exons. B and C: Pedigrees of DCM families carrying the R218W mutation (B; CM 2019 family) or L462P mutation (C; CM 2053 family) are shown. Filled square and filled circle indicate affected male and female, respectively. Open square and open circle represent unaffected male and female with DCM, respectively. Arrows indicate the proband patients. Presence (+) or absence (–) of the mutations is noted for analyzed individuals. II-3 in (C), who is represented by a shadowed circle, showed a regional hypokinesia in posterior ventricular wall. SD, sudden death. D: Alignment of amino acid sequences of BAG3 proteins from various species around the DCM-associated mutations, Arg218Trp (R218W) and Leu462Pro (L462P), along with polymorphisms identified in the Japanese populations. Protein sequence of human BAG3 predicted from the nucleotide sequences was aligned with that of rhesus monkey, cattle, rat, mouse, chicken, xenopus, and zebrafish.

Table 1. Clinical Characteristics of Individuals Carrying BAG3 Mutations

ID	Mutation	Age at exam (years) and gender	Age at onset (years)	LVDd (mm)	LVDs (mm)	IVST (mm)	PWT (mm)	%FS	%EF	Other remarks
CM2019 family II-1	R218W	76, male	73	54	48	10	10	11	29	ECG; ectopic atrial rhythm,
CM2053 family II-1	L462P	41, female	34	59	47	6	6	20	40	ECG; premature ventricular contraction, CK = 66 IU/l
CM2053 family II-3	L462P	27, female	27	48	31	7	6	35	64	EchoCG; partial hypokinesia in posterior ventricular wall, CK = 62 IU/l

LVDd, left ventricular end-diastolic dimension; LVDs, left ventricular end-systolic dimension; IVST, interventricular septum thickness; PWT, posterior wall thickness; %FS, percent fractional shortening; %EF, percent ejection fraction; ECG, electrocardiogram; EchoCG, echocardiogram; CK, creatine kinase.

cells transected with GFP-BAG3-WT showed similar morphological differentiation, because about half (40 to 50%) of myotubes transfected with GFP-BAG3-WT were over trinucleation (Fig. 4A–C). Similarly, after 5 days of differentiation, numbers of myotubes with over trinucleation were about half in cells transfected with GFP-BAG3-Arg218Trp (Fig. 4G–I), GFP-BAG3-Arg258Trp (Fig. 4J–L), and GFP-BAG3-Leu462Pro (Fig. 4M–O). In clear contrast, most (~90%) of myotubes transfected with GFP-BAG3-Pro209Leu were in binuclear state (Fig. 4D–F). These observations suggested that the MFM-associated mutation, Pro209Leu, might disturb the multinucleation during the differentiation into skeletal muscle myotubes. It should be noted that GFP-BAG3 proteins showed diffuse localization in the cytoplasm and did not show nuclear localization in the myotubes transfected with GFP-BAG3 constructs, even with the DCM-associated mutations (Fig. 4).

Altered Sensitivity to Apoptosis Caused by the DCM-Associated BAG3 Mutations

Because BAG3 is an antiapoptotic protein, we hypothesized that the *BAG3* mutations might render the cells susceptible to stress-induced apoptosis. To investigate the possible involvement of *BAG3* mutations in the abnormal regulation of cellular apoptosis, we first performed a TUNEL assay on NRCs transfected with GFP chimeras of *BAG3*. There was no difference in the frequency of TUNEL-positive cells among the nontransfected and transfected NRCs under the culture condition without serum starvation; less than 1% of NRCs were TUNEL positive. Under the serum-deprived condition for 24 hr, most (~90%) of NRCs expressing GFP-BAG3-WT showed negative TUNEL staining (Fig. 5A–C). In contrast, about half of NRCs transfected with GFP-BAG3-Arg218Trp (Fig. 5G–I) or GFP-BAG3-Leu462Pro (Fig. 5M–O) demonstrated positive TUNEL staining with disorganized GFP signals under the serum deprivation for 24 hr, albeit most (~90%) of NRCs transfected with GFP-BAG3-Pro209Leu (Fig. 5D–F) or GFP-BAG3-Arg258Trp (Fig. 5J–L) showed negative TUNEL staining with well-organized striated pattern of GFP signals. These observations indicate that the cardiomyopathy-associated *BAG3* mutations, but not the MFM-associated *BAG3* mutation or nondisease-related *BAG3* polymorphism, may increase the susceptibility to stress-induced apoptosis of NRCs.

To confirm the increased sensitivity to stress-induced apoptosis by the DCM-associated *BAG3* mutations by another method, we quantified apoptosis of H9c2 cells stably expressing GFP alone, GFP-BAG3-WT, or GFP chimera of each variant by the cell death ELISA assay. Stable transfected cell lines were treated with doxorubicin at the concentration of 1 μM for 24, 48, or 72 hr, and subjected to the assay. It was demonstrated that doxorubicin induced formation of oligonucleosomes in a time-dependent manner, and there was no significant difference among the nontransfected H9c2 cells and transfected cell lines expressing GFP only, GFP-BAG3-WT, GFP-BAG3-Pro209Leu, or GFP-BAG3-Arg258Trp (Fig. 6). On the other hand, significantly higher amounts of oligonucleosomes were observed in the stable transfectants expressing GFP-BAG3-Arg218Trp or GFP-BAG3-Leu462Pro than the transfectants expressing GFP-BAG3-WT, under the treatment by doxorubicin (Fig. 6). These observations further indicated that the DCM-associated *BAG3* mutations increased the sensitivities to apoptosis under the stressed condition.

Discussion

In the present study, we identified two DCM-associated mutations in a Z/I-band signaling protein, BAG3, which were not found in the controls and caused functional alterations. In addition, we found four other *BAG3* variations with amino acid replacements, but they were not considered to be associated with DCM, because they were present in the healthy individuals, even though evolutionary conserved residues were replaced. The DCM-associated mutations affected the Z-disc assembly of cardiomyocytes and increased the sensitivity to apoptosis under the metabolic stress. The latter functional change might be the reason for that the *BAG3* mutations were found in late-onset DCM. In other words, metabolic stresses to cardiomyocytes might be required to develop overt DCM in the subjects with the *BAG3* mutations found in this study.

We observed no functional alterations caused by the Arg258Trp variant in NRCs, a cardiomyocyte cell line H9c2, and a skeletal muscle cell line C2C12, suggesting that it was not a pathogenic mutation. Although the Arg258Trp mutation was recently reported in a Chinese patient with MFM, it was also found in the unaffected father of the patient and the patient carried another mutation Pro209Leu [Lee et al., 2011]. In this study, we demonstrated that the MFM-associated Pro209Leu mutation impaired the differentiation of skeletal muscle cell line C2C12, although it caused no functional alterations in the NRCs and in a cardiomyocyte cell line H9c2. The observations further suggested that the Arg258Trp variant was a simple polymorphism not associated with the diseases.

BAG3 is a co-chaperone protein and might not be directly involved in the muscle contractile function. Recent genetic studies have revealed that DCM is caused by the gene abnormalities not only in the cytoskeletal/contractile proteins, but also in the noncytoarchitectural molecules distributed in the Z/I-band region [Kimura, 2010]. We previously reported a DCM-associated Arg157His mutation in another chaperone protein, αB-crystallin, and this mutation did not show abnormal localization in the cytoplasm of NRC, whereas a myopathy-associated Arg120Gly mutation formed aggregated cytoplasmic depositions [Inagaki et al., 2006]. BAG3 and αB-crystallin bind with each other and both proteins serve to maintain protein homeostasis against the environmental stress [Hishiya

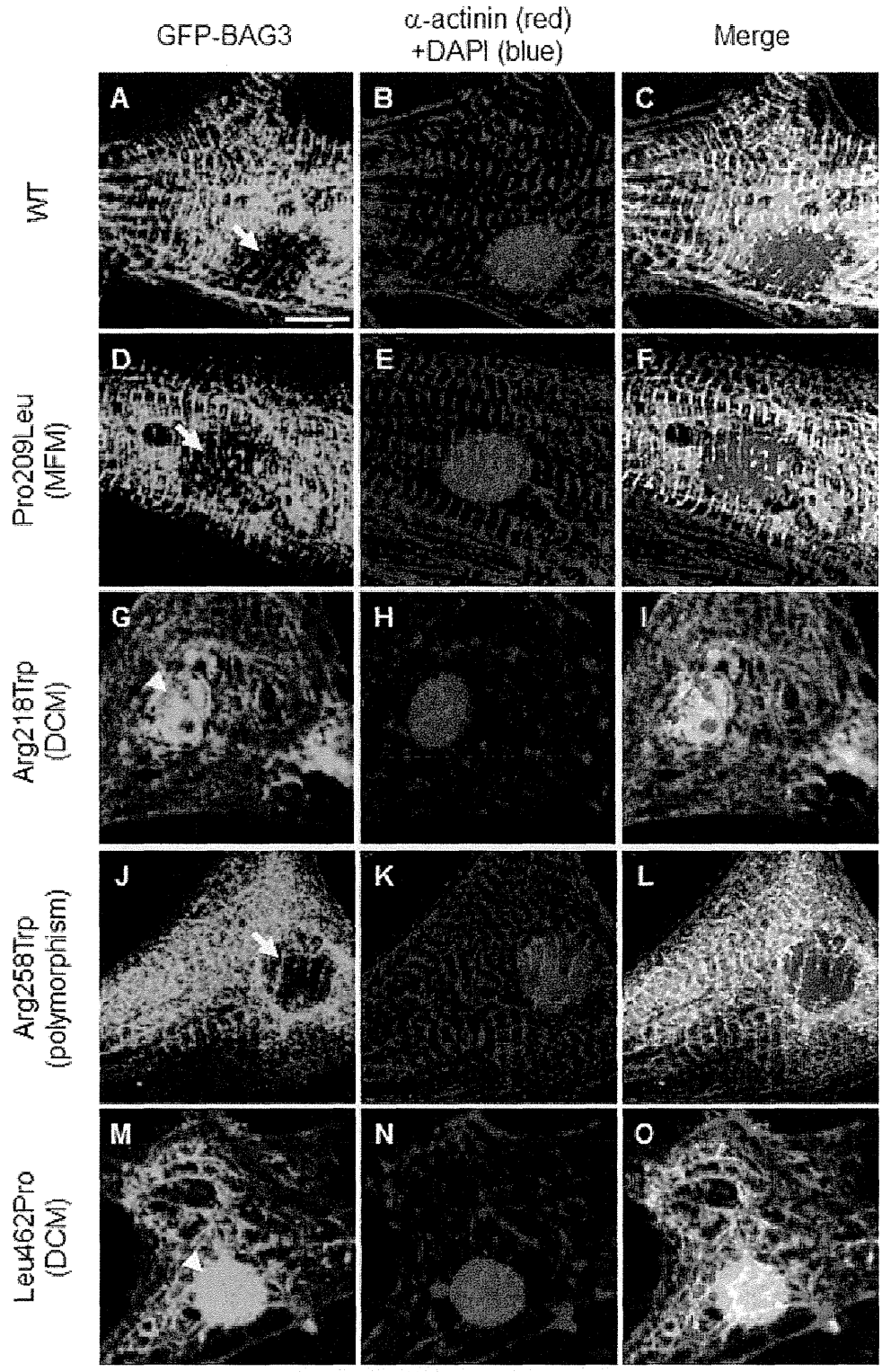

Figure 2. Distribution of α-actinin and transiently expressed GFP chimeras of *BAG3* in NRCs. NRCs transfected with GFP-tagged *BAG3* constructs for WT (A–C) or mutant (P209L, R218W, R258W, or L462P) (D–F, G–I, J–L, or M–O, respectively) were fixed 48 hr after the transfection, and stained with DAPI and anti-α-actinin antibody followed by secondary antibody (B, E, H, K, and N). Merged images are shown in C, F, I, L, and O. In the NRCs showing myofibrils with Z-discs, GFP-BAG3-WT is observed at the Z-discs and cytoplasm (A–C). GFP-tagged BAG3 proteins carrying the MFM-associated mutation, Pro209Leu, and nondisease-related variant, Arg258Trp, showed similar localization to that of WT (D–F and J–L, respectively). In contrast, GFP-tagged BAG3 proteins carrying the DCM-associated mutations, Arg218Trp and Leu462Pro, showed diffused localization that was associated with the disorganization of sarcomeric α-actinin (G–I and M–O). Arrows and arrowheads indicate the absence and presence, respectively, of GFP-BAG3 protein in nuclei. Scale bars = 10 μm.

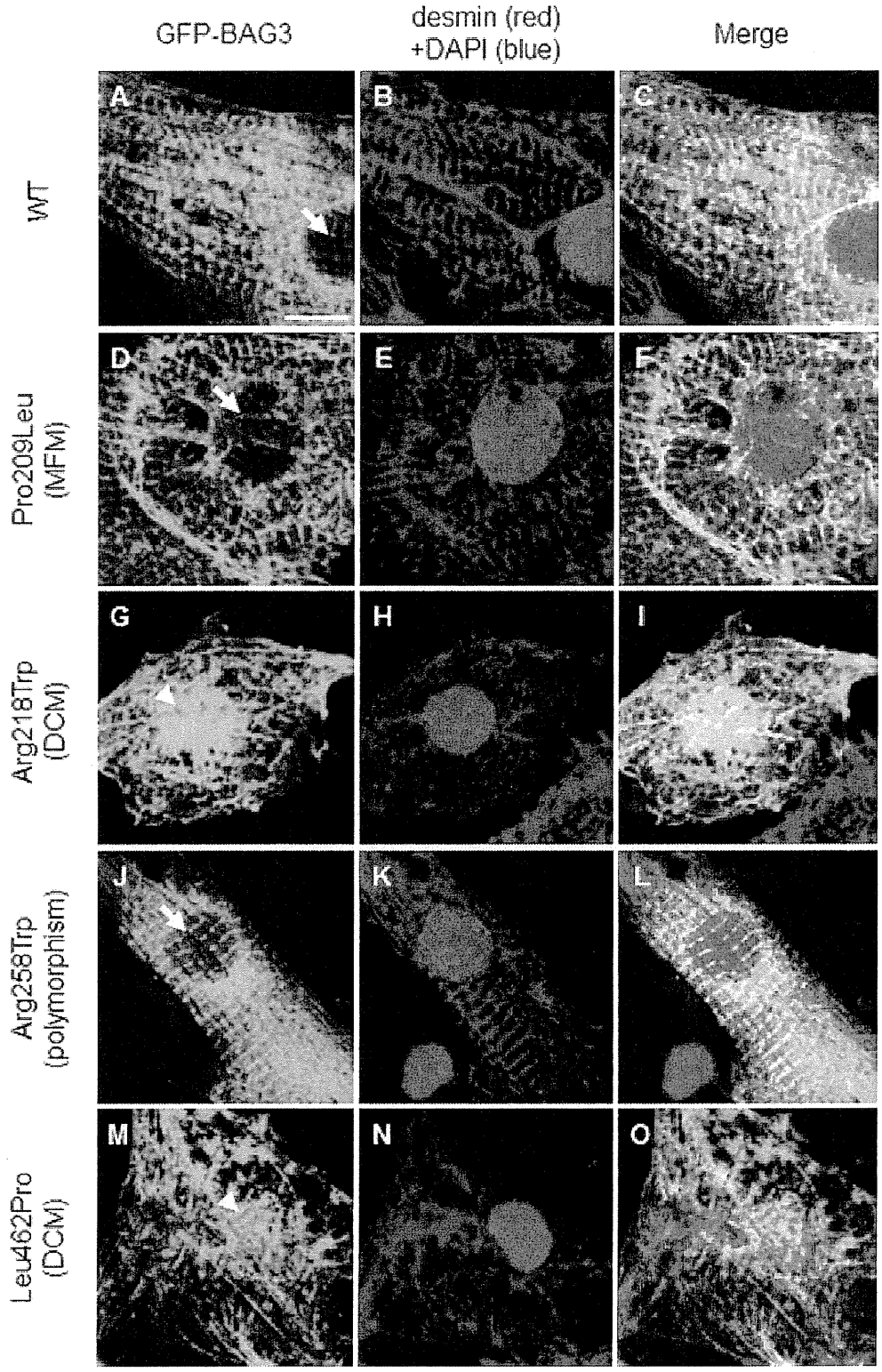

Figure 3. Distribution of desmin and transiently expressed GFP chimeras of BAG3 in NRCs. NRCs transfected with GFP-tagged BAG3 constructs for WT (A–C) or mutant (P209L, R218W, R258W, or L462P) (D–F, G–I, J–L, or M–O, respectively) were fixed 48 hr after the transfection, and stained with DAPI and anti-desmin antibody followed by secondary antibody (B, E, H, K, and N). Merged images are shown in C, F, I, L, and O. In the NRCs showing myofibrils with Z-discs, GFP-BAG3-WT is observed at the Z-discs and cytoplasm (A–C). GFP-tagged BAG3 proteins carrying the Pro209Leu and Arg258Trp, showed similar localization to that of WT (D–F and J–L, respectively). In contrast, GFP-tagged BAG3 proteins carrying the Arg218Trp and Leu462Pro, showed diffused localization that was associated with the disorganization of cytoskeletal desmin (G–I and M–O). Arrows and arrowheads indicate the absence and presence, respectively, of GFP-BAG3 in nuclei. Scale bars = 10 μm.

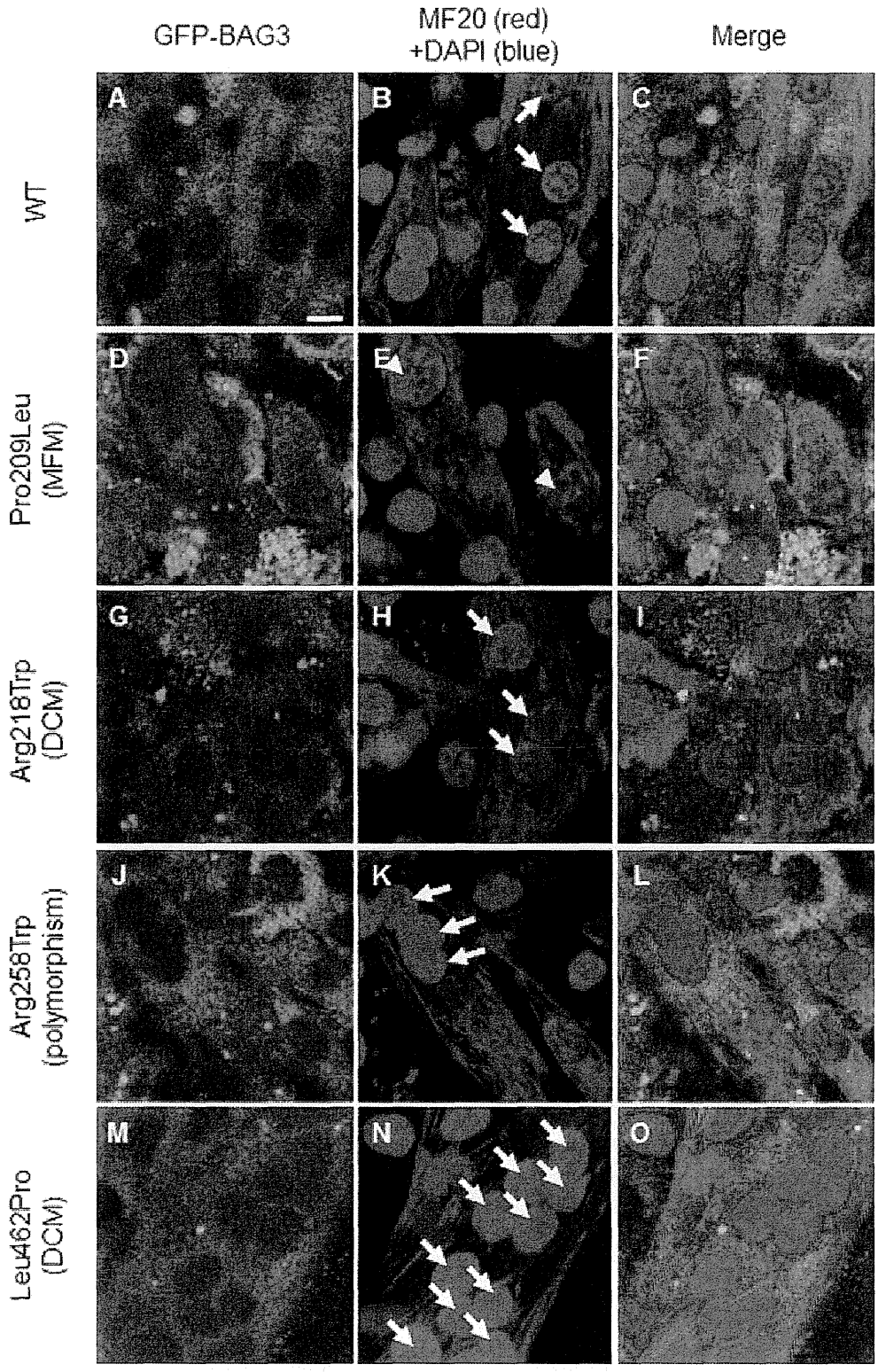

Figure 4. Differentiation of myoblasts into myotubes in C2C12 cells transiently expressed GFP chimeras of BAG3. C2C12 cells transfected with GFP-tagged BAG3 constructs for WT (A–C) or mutant (P209L, R218W, R258W, or L462P) (D–F, G–I, J–L, or M–O, respectively) were differentiated for 5 days in low-serum culture condition, and stained with DAPI and anti-MF20 antibody followed by secondary antibody (B, E, H, K, and N). Merged images are shown in C, F, I, L, and O. In the myotubes positively stained with MF20, GFP-BAG3 proteins were diffusely distributed in cytoplasm (A, D, G, I, and M). Trinucleations (arrows) were observed in the myotubes transfected with GFP- BAG3 WT, Arg218Trp, Arg258Trp, and Leu462Pro, but not in the myotubes transfected with GFP- BAG3 Pro209Leu (arrowheads). Scale bars = 10 μm. [Color figure can be viewed in the online issue, which is available at wiley.com/humanmutation.]

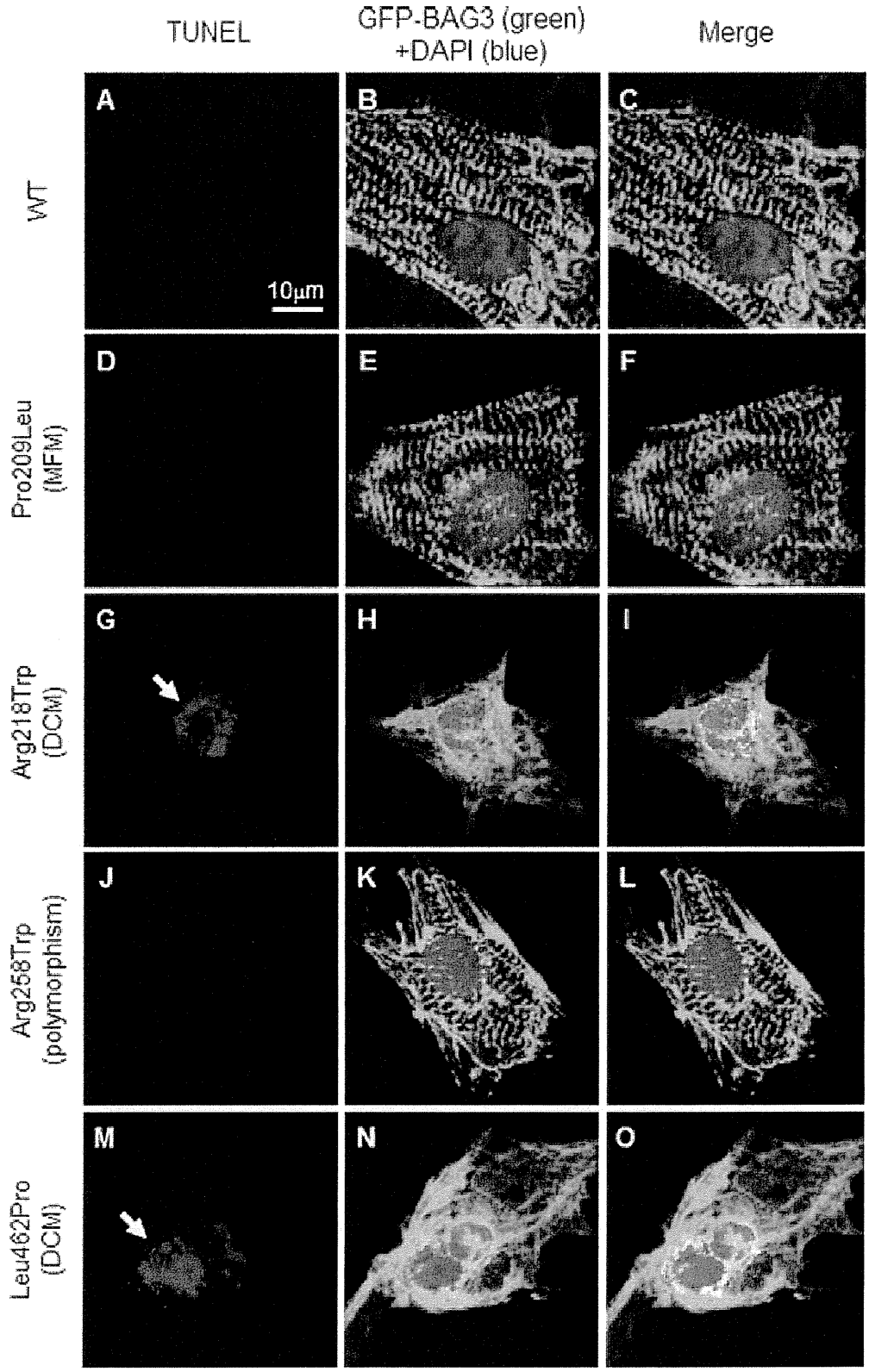

Figure 5. Apoptosis induced by serum deprivation in NRCs transfected with GFP-BAG3. NRCs were transfected with GFP chimeras of WT (A–C) or mutant (P209L, R218W, R258W, or L462P) (D–F, G–I, J–L, or M–O, respectively). The NRCs were cultured under FBS-free condition for additional 24 hr, fixed, subjected to the TUNEL assay, and stained with DAPI (B, E, H, K, and N). Merged images are shown in C, F, I, L, and O. Representative images of TUNEL assays are shown (A, D, G, J, and M). Arrows indicate apoptotic cells with positive TUNEL staining as visualized by red fluorescence; scale bars = 10 μm. [Color figure can be viewed in the online issue, which is available at wiley.com/humanmutation.]

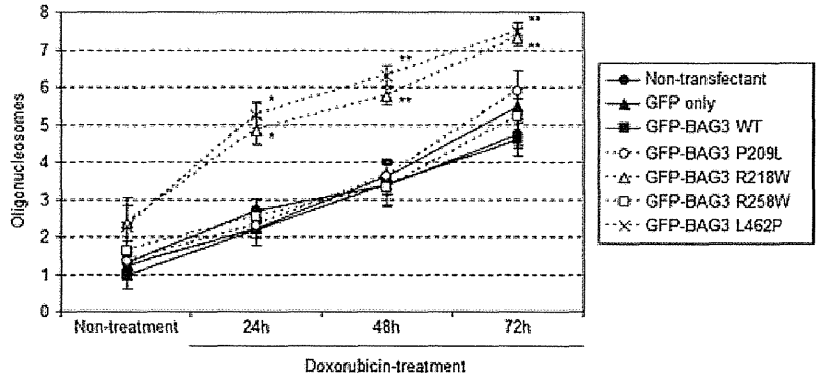

Figure 6. Quantitative analysis of apoptosis induced by doxorubicin in H9c2 cells stably expressing GFP-BAG3. H9c2 cells stably expressing each GFP chimera of *BAG3* in 96-well dishes were treated with 1 μM of doxorubicin for 24, 48, and 72 hr. Cell lysates were subjected to cell death ELISA assay. Amounts of mono- and oligonucleosomes were measured at 405 nm, and referenced by 490 nm. Data are arbitrarily expressed as means ± SEM ($n = 6$ for each case). * $P < 0.01$ versus WT; ** $P < 0.001$ versus WT.

et al., 2011]. In addition, they have crucial roles in protein folding, inhibition of protein aggregation, and degradation of misfolded proteins as chaperone-related proteins [Hishiya et al., 2011]. However, disrupted co-localization of BAG3 and α-actinin was observed for GFP-BAG3-Arg218Trp and GFP-BAG3-Leu462Pro without any cytoplasmic aggregation of mutant BAG3 proteins, indicating that the abnormal Z-disc assembly was directly associated with the *BAG3* mutations. It is worth noting that the functional alteration caused by the DCM-associated *BAG3* mutations was different from that by the DCM-associated αB-crystallin mutation, which was the decreased binding to titin N2-B region without disturbing the Z-disc assembly [Inagaki et al., 2006].

The mechanism of altered Z-disc assembly caused by the DCM-associated *BAG3* mutations is not clear, but a knockdown of *Bag3* in cardiomyocytes induced rapid myofibrillar degeneration and Z-disc disruption under the condition of mechanical stress [Hishiya et al., 2010], suggesting that *BAG3* might play a pivotal role in the Z-disc assembly during the myofibrillogenesis. In the transition from nascent to mature myofibrils, Z-disc precursors, Z-bodies, eventually fuse laterally to form Z-discs at the trunk of myocytes, which is accompanied by the induction of myofibrillar proteins, and this may stabilize the sarcomere structure required for muscle contraction. In this study, it was suggested that the DCM-associated mutations affected the assembly of sarcomere in NRCs. However, because we did not assessed the turnover and/or reorganization of the Z-discs, molecular mechanisms of disturbing the Z-disc organization during myofibrillogenesis should be further investigated in future studies.

The myofibrillar integrity under mechanical stress is maintained by the BAG3–Hsc70 interaction [Hishiya et al., 2010], and Hsc70 is a regulator of a chaperone-dependent E3 ligase CHIP [Murata et al., 2003; Pratt et al., 2010]. It was reported that CHIP-mediated degradation of p53 was involved in the protection against myocardial damage under ischemic condition [Naito et al., 2011]. These observations imply a possible link between the myofibrinogenesis and stress-induced apoptosis of cardiomyocytes. It is well known that serum deprivation and doxorubicin induce apoptosis of cultured cardiomyocytes including NRCs [Chao et al., 2005] and H9c2 cells [Chua et al., 2006], and we demonstrated that the DCM-associated *BAG3* mutations increased the sensitivity to apoptosis of the cardiomyocytes under the stressed conditions. Because BAG3 protein possess antiapoptotic function by enhancing the activity of bcl-2 [Lee et al., 1999], increased number of TUNEL-positive cells and oligonucleosomes in NRCs and H9c2 cells, respectively, expressing the DCM-associated *BAG* mutations might be due to the impaired function of BAG3 protein. Quite interestingly, we observed nuclear localization of GFP-BAG3-Arg218Trp and GFP-BAG3-Leu462Pro proteins in NRCs. Because the abnormal intranuclear accumulation was not observed in the NRCs transfected with GFP-BAG3-WT, GFP-BAG3-Pro209Leu, or GFP-BAG3-Arg258Trp, recruitment of BAG3 protein into nuclei may be a specific phenomenon caused by the DCM-associated mutations, which might be involved in the apoptosis of cardiomyocytes leading to DCM. Because the nuclear localization of mutant GFP-BAG3 proteins was observed in both apoptotic and nonapoptotic cells, we could not conclude whether the apoptosis was a direct consequence of the nuclear localization of mutant GFP-BAG3 proteins. Additional studies will be required to clarify the issue.

A number of skeletal muscle diseases and isolated DCM are caused by mutations in the same genes [Arimura et al., 2007]. The patients with muscular diseases often suffer from cardiac involvement, but most of the patients with isolated DCM do not manifest with the skeletal muscle phenotype. The etiological link between the inherited skeletal muscle diseases and hereditary DCM has raised a question as how the mutations in the genes/proteins expressed in both skeletal and cardiac muscles cause heart-specific phenotypes in the isolated DCM. The most probable explanation was that the phenotypic differences between the skeletal muscle disease and DCM might be due to that mutations in specific and/or different functional domains would affect specific functions. In this study, we found that the MFM-associated mutation, Pro209Leu, did not affect either the Z-disc assembly or the sensitivity to apoptosis. In clear contrast, the DCM-associated Arg218Trp mutations, which located near the Pro209Leu mutation, and the other DCM-associated Leu462Pro mutation caused abnormalities in both Z-disc assembly and sensitivity to apoptosis. It was reported that BAG3 protein with the Pro209Leu mutation was found predominantly in the abnormal form of small discrete granules in the COS-7 cells [Selcen et al., 2009], but such abnormality was not observed in NRCs, H9c2 cells, and C2C12 cells in this study. The reason why the Pro209Leu mutation did not show aggregations in the cardiomyocytes and skeletal muscle cell line is not clear, but the COS-7 cells are used for overexpression of genes from transfected constructs containing the replication origin of SV40, raising a possibility that the aggregation

was caused by the overexpression of mutant BAG3 proteins in the COS-7 cells.

The MFM patients carrying the Pro209Leu mutation were reported to demonstrate cardiac phenotypes of hypertrophic and/or restrictive cardiomyopathy, which are different from DCM. It is notable that the MFM patients manifested with cardiac phenotypes of early onset in childhood. Because the patients carrying the Arg218Trp or Leu462Pro mutations suffered from adult-onset DCM (Table 1), it was speculated that the pathological mechanisms of *BAG3* mutations might be different between the cardiomyopathy accompanied by MFM and isolated DCM. We demonstrated that the MFM-associated Pro209Leu mutation impaired the formation of multinuclear myotubes during the differentiation of C2C12 cells, which was not found with the DCM-associated mutations. However, this functional deficit may not associate with the cardiac phenotype caused by the Pro209Leu mutation, because cell fusion during the differentiation is specific to skeletal muscle cells and not found in cardiomyocytes. On the other hand, disturbance of myotube formation by the Pro209Leu mutation might be an underlying mechanism leading to skeletal muscle phenotypes in MFM, although it is not clear how the Pro209Leu mutation causes axonal neuropathy with giant axons [Odgerel et al., 2010]. Further studies will be required to reveal the difference in the molecular mechanisms of disease phenotypes caused by the *BAG3* mutations.

In conclusion, we report here two heterozygous missense mutations of *BAG3* found in familial DCM, which cause abnormal Z-disc assembly and increase the sensitivity to apoptosis in the cardiomyocytes. We demonstrate here for the first time the association between DCM and increased sensitivity to apoptosis accompanied by the abnormality in myofibrillogenesis. However, the overexpression of mutant proteins in cultured cardiac myocytes has significant limitation to mimic the situation in intact hearts. Further studies on the functional role of BAG3 protein in the cardiac muscle will help understanding the association between the abnormal function of BAG3 protein and DCM.

Acknowledgments

Conflict of Interest: None declared.

References

Arimura T, Bos JM, Sato A, Kubo T, Okamoto H, Nishi H, Harada H, Koga Y, Moulik M, Doi YL, Towbin JA, Ackerman MJ, Kimura A. 2009. Cardiac ankyrin repeat protein gene (ANKRD1) mutations in hypertrophic cardiomyopathy. J Am Coll Cardiol 54: 334–342.

Arimura T, Hayashi T, Kimura A. 2007. Molecular etiology of idiopathic cardiomyopathy. Acta Myol 26: 153–158.

Chao W, Shen Y, Zhu X, Zhao H, Novikov M, Schmidt U, Rosenzweig A. 2005. Lipopolysaccharide improves cardiomyocyte survival and function after serum deprivation. J Biol Chem 280: 21997–22005.

Chua CC, Liu X, Gao J, Hamdy RC, Chua BH. 2006. Multiple actions of pifithrin-alpha on doxorubicin-induced apoptosis in rat myoblastic H9c2 cells. Am J Physiol Heart Circ Physiol 290: H2606–H2613.

Hayashi T, Arimura T, Itoh-Satoh M, Ueda K, Hohda S, Inagaki N, Takahashi M, Hori H, Yasunami M, Nishi H, Koga Y, Nakamura H, Matsuzaki M, Choi BY, Bae SW, You CW, Han KH, Park JE, Knoll R, Hoshijima M, Chien KR, Kimura A. 2004. Tcap gene mutations in hypertrophic cardiomyopathy and dilated cardiomyopathy. J Am Coll Cardiol 44: 2192–2201.

Hishiya A, Kitazawa T, Takayama S. 2010. BAG3 and Hsc70 interact with actin capping protein CapZ to maintain myofibrillar integrity under mechanical stress. Circ Res 107: 1220–1231.

Hishiya A, Salman MN, Carra S, Kampinga HH, Takayama S. 2011. BAG3 directly interacts with mutated alphaB-Crystallin to suppress its aggregation and toxicity. PLoS One 6: e16828.

Homma S, Iwasaki M, Shelton GD, Engvall E, Reed JC, Takayama S. 2006. BAG3 deficiency results in fulminant myopathy and early lethality. Am J Pathol 169: 761–773.

Inagaki N, Hayashi T, Arimura T, Koga Y, Takahashi M, Shibata H, Teraoka K, Chikamori T, Yamashina A, Kimura A. 2006. Alpha B-crystallin mutation in dilated cardiomyopathy. Biochem Biophys Res Commun 342: 379–386.

Kimura A. 2010. Molecular basis of hereditary cardiomyopathy: abnormalities in calcium sensitivity, stretch response, stress response and beyond. J Hum Genet 55: 81–90.

Lee H, Cherk S, Chan S, Wong S, Tong T, Ho W, Chan A, Lee K, Mak C. 2011. BAG3-related myofibrillar myopathy in a Chinese family. Clin Genet, doi: 10.1111/j.1399-0004.2011.01659.x. [Epub ahead of print]

Lee JH, Takahashi T, Yasuhara N, Inazawa J, Kamada S, Tsujimoto Y. 1999. Bis, a Bcl-2-binding protein that synergizes with Bcl-2 in preventing cell death. Oncogene 18: 6183–6190.

Maron BJ, Towbin JA, Thiene G, Antzelevitch C, Corrado D, Arnett D, Moss AJ, Seidman CE, Young JB. 2006. Contemporary definitions and classification of the cardiomyopathies: an American Heart Association Scientific Statement from the Council on Clinical Cardiology, Heart Failure and Transplantation Committee; Quality of Care and Outcomes Research and Functional Genomics and Translational Biology Interdisciplinary Working Groups; and Council on Epidemiology and Prevention. Circulation 113: 1807–1816.

Murata S, Chiba T, Tanaka K. 2003. CHIP: a quality-control E3 ligase collaborating with molecular chaperones. Int J Biochem Cell Biol 35: 572–578.

Naito AT, Okada S, Minamino T, Iwanaga K, Liu ML, Sumida T, Nomura S, Sahara N, Mizoroki T, Takashima A, Akazawa H, Nagai T, Shiojima I, Komuro I. 2010. Promotion of CHIP-mediated p53 degradation protects the heart from ischemic injury. Circ Res 106: 1692–1702.

Norton N, Li D, Rieder MJ, Siegfried JD, Rampersaud E, Zuchner S, Mangos S, Gonzalez-Quintana J, Wang L, McGee S, Reiser J, Martin E, Nickerson DA, Hershberger RE. 2011. Genome-wide studies of copy number variation and exome sequencing identify rare variants in BAG3 as a cause of dilated cardiomyopathy. Am J Hum Genet 88: 273–282.

Odgerel Z, Sarkozy A, Lee HS, McKenna C, Rankin J, Straub V, Lochmüller H, Paola F, D'Amico A, Bertini E, Bushby K, Goldfarb LG. 2010. Inheritance patterns and phenotypic features of myofibrillar myopathy associated with a BAG3 mutation. Neuromuscul Disord 20: 438–442.

Pratt WB, Morishima Y, Peng HM, Osawa Y. 2010. Proposal for a role of the Hsp90/Hsp70-based chaperone machinery in making triage decisions when proteins undergo oxidative and toxic damage. Exp Biol Med 235: 278–289.

Selcen D, Muntoni F, Burton BK, Pegoraro E, Sewry C, Bite AV, Engel AG. 2009. Mutation in BAG3 causes severe dominant childhood muscular dystrophy. Ann Neurol 65: 83–89.

Takayama S, Xie Z, Reed JC. 1999. An evolutionarily conserved family of Hsp70/Hsc70 molecular chaperone regulators. J Biol Chem 274: 781–786.

Villard E, Perret C, Gary F, Proust C, Dilanian G, Hengstenberg C, Ruppert V, Arbustini E, Wichter T, Germain M, Dubourg O, Tavazzi L, Aumont MC, Degroote P, Fauchier L, Trochu JN, Gibelin P, Aupetit JF, Stark K, Erdmann J, Hetzer R, Roberts AM, Barton PJ, Regitz-Zagrosek V, Aslam U, Duboscq-Bidot L, Meyborg M, Maisch B, Madeira H, Waldenstrom A, Galve E, Cleland JG, Dorent R, Roizes G, Zeller T, Blankenberg S, Goodall AH, Cook S, Tregouet DA, Tiret L, Isnard R, Komajda M, Charron P, Cambien F. A genome-wide association study identifies two loci associated with heart failure due to dilated cardiomyopathy. Eur Heart J 32: 1065–1076.

Cell Calcium 55 (2014) 17–23

Contents lists available at ScienceDirect

Cell Calcium

journal homepage: www.elsevier.com/locate/ceca

Genetic modulation of the SERCA activity does not affect the Ca^{2+} leak from the cardiac sarcoplasmic reticulum

Satoshi Morimoto[a], Kenichi Hongo[a,*], Yoichiro Kusakari[b], Kimiaki Komukai[a], Makoto Kawai[a], Jin O-Uchi[c], Hiroyuki Nakayama[d], Michio Asahi[e], Kinya Otsu[f], Michihiro Yoshimura[a], Satoshi Kurihara[b]

[a] Division of Cardiology, Department of Internal Medicine, The Jikei University School of Medicine, Tokyo, Japan
[b] Department of Cell Physiology, The Jikei University School of Medicine, Tokyo, Japan
[c] Center for Translational Medicine, Department of Medicine, Jefferson Medical College, Thomas Jefferson University, Philadelphia, USA
[d] Department of Clinical Pharmacology and Pharmacogenomics, Graduate School of Pharmaceutical Sciences, Osaka University, Osaka, Japan
[e] Department of Pharmacology, Faculty of Medicine, Osaka Medical College, Osaka, Japan
[f] Cardiovascular Division, King's College London, London, United Kingdom

ARTICLE INFO

Article history:
Received 15 June 2013
Received in revised form 25 October 2013
Accepted 28 October 2013
Available online 13 November 2013

Keywords:
Cardiac muscle
Excitation-contraction coupling
Aequorin
Ca^{2+} transient
Transgenic mouse

ABSTRACT

The Ca^{2+} content in the sarcoplasmic reticulum (SR) determines the amount of Ca^{2+} released, thereby regulating the magnitude of Ca^{2+} transient and contraction in cardiac muscle. The Ca^{2+} content in the SR is known to be regulated by two factors: the activity of the Ca^{2+} pump (SERCA) and Ca^{2+} leak through the ryanodine receptor (RyR). However, the direct relationship between the SERCA activity and Ca^{2+} leak has not been fully investigated in the heart. In the present study, we evaluated the role of the SERCA activity in Ca^{2+} leak from the SR using a novel saponin-skinned method combined with transgenic mouse models in which the SERCA activity was genetically modulated. In the SERCA overexpression mice, the Ca^{2+} uptake in the SR was significantly increased and the Ca^{2+} transient was markedly increased. However, Ca^{2+} leak from the SR did not change significantly. In mice with overexpression of a negative regulator of SERCA, sarcolipin, the Ca^{2+} uptake by the SR was significantly decreased and the Ca^{2+} transient was markedly decreased. Again, Ca^{2+} leak from the SR did not change significantly. In conclusion, the selective modulation of the SERCA activity modulates Ca^{2+} uptake, although it does not change Ca^{2+} leak from the SR.

1. Introduction

Cardiac muscle contraction is regulated by Ca^{2+} released from intracellular Ca^{2+} stores in a region named the sarcoplasmic reticulum (SR), a central player in excitation–contraction coupling that allows actin–myosin interactions to produce active tension [1]. Membrane depolarization opens L-type Ca^{2+} channels, thereby leading to Ca^{2+} influx through the sarcolemma. A small increase in $[Ca^{2+}]_i$ due to Ca^{2+} influx can trigger a large amount Ca^{2+} release from the SR through the Ca^{2+} release channel (ryanodine receptor, RyR) which is known as the Ca^{2+}-induced Ca^{2+} release mechanism [2]. The amplitude of the intracellular Ca^{2+} transient, which determines cardiac contractility, is largely dependent on the Ca^{2+} content in the SR [1]. Two important regulators of the Ca^{2+} content in the SR are the activity of the Ca^{2+} pump (sarco/endoplasmic reticulum Ca^{2+}-ATPase, SERCA), which actively transports Ca^{2+} from the myoplasm to inside the SR, and Ca^{2+} leak through the RyR. The amount of Ca^{2+} released from the SR is known to exhibit a steep relationship with the Ca^{2+} content in the SR, and a small change in the Ca^{2+} content can produce a large change in the amount of Ca^{2+} released [3]. This mechanism is thought to be important for changes in the activity of SERCA to modulate $[Ca^{2+}]_i$. Recent studies revealed that changes in the amount of Ca^{2+} leak through the RyR also regulate the Ca^{2+} content and the amplitude of $[Ca^{2+}]_i$ under both physiological and pathophysiological conditions [4,5]. Under physiological conditions, Ca^{2+} leak occurs during diastole and can prevent Ca^{2+} overload upon the increased Ca^{2+} cycling (such as sympathetic nervous stimulation) [5]. Moreover, a recent report suggested that differences in the amount of Ca^{2+} leak can explain the strain differences observed in Ca^{2+} handling among mouse strains [6]. Under pathophysiological conditions, such as heart failure, excess Ca^{2+} leak from the SR decreases the Ca^{2+} content in the SR and hence reduces the amount of Ca^{2+} available to produce cardiac contractions, possibly due to the phosphorylation

* Corresponding author at: Division of Cardiology, Department of Internal Medicine, The Jikei University School of Medicine, 3-25-8 Nishi-shimbashi, Minato-ku, Tokyo 105-8461, Japan. Tel.: +81 3 3433 1111; fax: +81 3 3459 6043.
E-mail address: hongo@jikei.ac.jp (K. Hongo).

0143-4160/$ – see front matter © 2013 Elsevier Ltd. All rights reserved.
http://dx.doi.org/10.1016/j.ceca.2013.10.005

of the RyR [4,7]. Although these two regulators (the SERCA activity and Ca^{2+} leak) are important for modulating cardiac contractility, the direct relationship between the SERCA activity and Ca^{2+} leak has not been fully investigated due to the lack of ideal models to estimate these two activities separately in the same experimental sample and the difficulty of selectively modulating the SERCA activity *in vitro*. The Ca^{2+} leak function has been investigated in single cardiomyocytes using Ca^{2+} spark measurement [8] and pharmacological inhibition of Ca^{2+} leak [7] and in the lipid bilayer using electrical Ca^{2+} flux measurement [9]. In contrast, the Ca^{2+} uptake function has been estimated in microsomal fraction-enriched SR using fluorescence dye or radioisotopes [10]. Therefore, it is difficult to estimate Ca^{2+} uptake and Ca^{2+} leak separately in the same experimental sample using the above methods.

Recently, we reported a novel method to estimate Ca^{2+} uptake and Ca^{2+} leak separately in the same preparation using saponin-skinned mouse left ventricular preparations [5]. We also created two transgenic mouse models of selectively increasing or decreasing the SERCA activity [10,11]. In the present study, we investigated the direct interaction between the SERCA activity and Ca^{2+} leak using the saponin-skinned method combined with transgenic mouse models in which the SERCA activity was selectively modulated. We also determined the changes in the level of $[Ca^{2+}]_i$ and contractions in these transgenic mouse models to estimate the relationship between the SERCA activity and Ca^{2+} leak under beat to beat conditions.

2. Materials and methods

2.1. Animals

All experiments were performed in accordance with the Guidelines on Animal Experimentation of The Jikei University School of Medicine. The study protocol was approved by the Animal Care Committee of The Jikei University School of Medicine (Approval number: 19-049C1). The investigation conformed to the Guidelines for the Care and Use of Laboratory Animals published by the US National Institutes of Health (NIH Publication No. 85-23, revised 1996).

Transgenic (TG) mice with cardiac-specific overexpression of rabbit cardiac SERCA (SERCA-TG) were generated under the control of the cardiac α-MHC gene promoter in the C57BL/6 background using the same procedure we previously employed to generate mutant SERCA2 (K397/400E)-overexpression mice [10]. Genotyping was performed to identify mice with the transgene using the following primers: 5′-AGG AGA AGG ACG GAC AAG GA-3′ and 5′-TGG AGG AGG TGG CAG AAA CA-3′. Non-transgenic littermate (NTG) mice were used as controls. The SERCA-TG mice were born in the expected Mendelian ratios and had a normal life span as wild-type mice.

The generation of mice with a cardiac-specific overexpression of sarcolipin (SLN-TG) has been previously reported [11]. Briefly, flag-tagged SLN was overexpressed under the control of the cardiac β-MLC gene promoter in the FVB background, and genotyping was performed in the mice with flag-tagged SLN using the following primers: 5′-CAG CCT CTG CTA CTC CTC TTC CTG CCT GTT C-3′ and 5′-GTA GGA CCT CAC AAG GAG CCA AAT AAG-3′. NTG mice were also used as control. The SLN-TG mice were born in the expected Mendelian ratios and had a normal life span compared with wild-type mice. The left ventricular pressure and heart rate values were also the same between the SLN-TG mice and NTG mice (data not shown). No major Ca^{2+} handling proteins, including SERCA, were altered. The SERCA activity was significantly decreased in the SLN-TG mice hearts, without changes in sensitivity to the Ca^{2+} concentration, as previously described [11].

2.2. Preparations

The papillary muscles or trabeculae dissected from the left ventricle of 10- to 12-week-old mice were used for the experiments [5,12]. The hearts were quickly removed from mice anesthetized with sodium pentobarbital (200–300 mg/kg i.p.). The aorta was cannulated with a blunted 18 G needle, and the heart was mounted on a Langendorff apparatus perfused with Tyrode's solution containing 2 mmol/L of Ca^{2+} at constant pressure for five minutes [5,12]. The heart beat was completely stopped by changing the solution to a solution containing 20 mmol/L of 2, 3-butanedione monoxime (BDM) (Nacalai Tesque, Inc., Kyoto, Japan). The left ventricle was opened, and the papillary muscles or thin trabeculae were dissected.

2.3. Measurement of intracellular Ca^{2+} transient and isometric tension

A Ca^{2+} sensitive photoprotein aequorin was used to measure the intracellular Ca^{2+} transient (CaT) simultaneously with isometric tension in the left ventricular papillary muscle preparations [12]. The aequorin was microinjected into 50–100 superficial cells of each preparation by applying high pressure with nitrogen gas using glass micropipettes. The preparation was electrically stimulated with platinum electrodes (1 mmol/L Ca^{2+}, 0.5 Hz, 30 °C) and the evoked aequorin light signal was recorded using a photomultiplier (EMI9789A, Ruislip, UK) simultaneously with measurement of the isometric tension (BG-10, Kulite, NJ, USA). The aequorin light signals were averaged and converted to the intracellular Ca^{2+} concentration using *in vitro* calibration [13].

2.4. Measurement of the Ca^{2+} content in the SR

The method used to estimate the SR function has been previously reported (Supplementary Figure I) [5] [14]. Briefly, the papillary muscles or trabeculae were cut along the longitudinal axis (≅200 μm × 2–5 mm) in the experimental solution and both ends of the preparation were tied to a tungsten wire with silk threads. Then, the preparation was permeabilized with saponin (50 μg/ml) in the relaxing solution for 30 minutes and inserted into a glass capillary tube placed on an inverted microscope (Nikon, Tokyo, Japan). An excitation light wavelength of 488 nm and emission wavelength of longer than 510 nm through a cut-off filter (DM-510, Nikon, Tokyo, Japan) were used to monitor the fluorescence signal of fluo-3 (Dojindo Laboratories, Kumamoto, Japan) using a fluorometry system (CAM-230, JASCO, Tokyo, Japan).

In the Ca^{2+} uptake assay (Supplementary Figure IA–D), after the SR was loaded with Ca^{2+} by activating SERCA with adenosine triphosphate (ATP) (4 mmol/L), caffeine (50 mmol/L) was applied to release the accumulated Ca^{2+} from the SR into the experimental solution containing fluo-3 (30 μM). As fluo-3 predominantly binds most of the Ca^{2+} released from the SR, the fluo-3 fluorescence change upon Ca^{2+} binding provides an estimate of the amount of accumulated Ca^{2+} in the SR before caffeine application. In the Ca^{2+} leak assay (Supplementary Figure IE–H), the preparation was perfused with the experimental solution containing ethylene glycol bis[β-aminoethylether]-N, N, N′,N′-tetraacetic acid (EGTA) (1 mmol/L) for various durations following Ca^{2+} loading, and then the remaining Ca^{2+} was measured using the same protocol. We then estimated the maximal Ca^{2+} content, which reflects the level of Ca^{2+} fully-loaded in the SR, by extrapolating of the sampling point of each Ca^{2+} content to reach the Ca^{2+} content at time zero. The amount of Ca^{2+} leak was estimated by subtracting the remaining Ca^{2+} content from the maximal Ca^{2+} content (see the Supplementary Data for details).

2.5. Solutions and chemicals

Tyrode's solution buffered with N-2-hydroxyethyl-piperazine-N-2-ethanesulfonic acid (HEPES) was used for Langendorff perfusion of the hearts, dissection of the preparations and the aequorin experiment. The composition of the Tyrode's solution was as follows: 136.9 mmol/L of NaCl, 5.4 mmol/L of KCl, 0.5 mmol/L of $MgCl_2$, 1–2 mmol/L of $CaCl_2$, 0.33 mmol/L of $NaHPO_4$, 5 mmol/L of HEPES and 5 mmol/L of glucose. The pH was adjusted to 7.40 ± 0.05 with NaOH at 30 °C, and the solution was equilibrated with 100% O_2.

The solutions used to estimate the SR function was based on potassium methanesulfonate (KMS) (103–164 mmol/L) to maintain a constant ionic strength under various conditions. The Ca^{2+} concentration was below pCa 8, except for the "loading" period (between pCa 8 and pCa 5.6). The experimental solution contained 20 mmol/L of NaN_3 to block the Ca^{2+} uptake in the mitochondria and 20 mmol/L of piperazine-N-N′-bis[2-ethanesulfonic acid] (PIPES) (ionic strength, 0.2 mol/L; temperature, 22 °C; pH adjusted with KOH). ATP (4 mmol/L) was present during the "load" period to activate the SERCA in the loading step. Each assay solution contained 50 mmol/L of caffeine and 25 mmol/L of adenosine-5′-monophosphate (AMP) to open the Ca^{2+} release channel (RyR) of the SR effectively. Fluo-3 was added to the "pre-assay" and "assay" solutions at a final concentration of 30 μM [5,14] (see Supplementary Table 1 for details).

All reagents were purchased from Sigma-Aldrich (Saint Louis, MO), unless otherwise indicated.

2.6. Statistics

All measured data are presented as the means ± standard error of the mean (SEM). Statistical significance was estimated using the unpaired Student's *t*-test for two sets of data and using a one-way analysis of variance (ANOVA) followed by the Bonferroni *post hoc* test for multiple comparisons, with the significance level set at $p < 0.05$. All statistical analyses were performed using the SPSS software program version 11.5 (SPSS Inc., Chicago, IL, USA).

3. Results

3.1. Protein expression levels and hemodynamics of the SERCA-TG mice

In the hearts of the SERCA-TG mice, the SERCA protein levels were significantly increased (1.68 ± 0.10-fold increase) compared to those observed in the NTG mice, as demonstrated by Western immunoblotting ($n = 3$ for SERCA-TG, $n = 3$ for NTG) (Supplementary Figure II). No other major Ca^{2+} handling proteins were altered. The left ventricular pressure and heart rate values were the same between the SERCA-TG mice and NTG mice ($n = 6$ for SERCA-TG, $n = 6$ for NTG) (Supplementary Figure III).

3.2. Effects of selective upregulation of the SERCA activity on the Ca^{2+} transient and isometric tension in the intact preparations

First, we investigated the Ca^{2+} handling and contractions in the SERCA-TG heart. We evaluated the Ca^{2+} transient and isometric tension under field stimulation at 0.5 Hz, because the contractility of the isolated muscle preparation is stable at a lower stimulation frequency during the long period of the experiments [12]. However, we also evaluated these under a higher stimulation frequency (up to 2 Hz) and found similar results to those observed at 0.5 Hz (data not shown). The left graphs of Fig. 1 present representative traces of the Ca^{2+} transient (A) and isometric tension (B) recorded from the intact papillary muscle preparations of the SERCA-TG and NTG hearts. The peaks of the Ca^{2+} transient and isometric tension were significantly increased in the SERCA-TG hearts compared to that observed in the NTG hearts ($p < 0.05$) ($n = 6$ for SERCA-TG, $n = 8$ for NTG). The time to reach the peak of the Ca^{2+} transient (TP) did not change significantly; however, the decay time of the Ca^{2+} transient from the peak to half of the peak (DT) was significantly shortened in the SERCA-TG hearts ($p < 0.01$). Both the time to reach the peak of tension (TPT) ($p < 0.01$) and the relaxation time from the peak tension to half the peak (RT) ($p < 0.01$) were significantly shortened in the SERCA-TG hearts.

3.3. Effects of selective upregulation of the SERCA activity on the SR function in the saponin-treated preparations

We then estimated the SR function in the SERCA-TG hearts. Fig. 2A shows the time-dependent changes in Ca^{2+} uptake into the SR estimated in the loading solution at pCa 7 using the saponin-skinned preparations ($n = 13$ for SERCA-TG, $n = 8$ for NTG). The amount of Ca^{2+} uptake was significantly accelerated in the early phase (less than 10 s) of Ca^{2+} loading in the SERCA-TG hearts. Fig. 2B shows the Ca^{2+}-dependent changes in the Ca^{2+} uptake estimated at the early phase of Ca^{2+} loading ($n = 16$ for SERCA-TG, $n = 16$ for NTG). At the fixed loading time of 10 s, the amount of Ca^{2+} uptake into the SR was significantly increased between pCa 7.4 and pCa 6.6 in the SERCA-TG hearts. The maximal Ca^{2+} content was estimated in the SERCA-TG and NTG hearts. As shown in Fig. 2C, the maximal Ca^{2+} content in the SERCA-TG hearts was not significantly different from that observed in the NTG hearts ($n = 29$ for SERCA-TG, $n = 24$ for NTG).

Finally, we investigated Ca^{2+} leak from the SR under the selective overexpression of SERCA. Fig. 2D shows the time-dependent changes in Ca^{2+} leak from the SR ($n = 29$ for SERCA-TG, $n = 24$ for NTG). The time course of Ca^{2+} leak was identical between the SERCA-TG and NTG hearts.

3.4. Effects of selective downregulation of the SERCA activity on the Ca^{2+} transient and isometric tension in the intact preparations

In the next series of experiments, we investigated the role of the selective downregulation of SERCA on excitation-contraction coupling using SLN-TG hearts. We first estimated the Ca^{2+} transient and isometric tension of the intact papillary muscle preparations obtained from the SLN-TG and NTG mice. The left graphs of Fig. 3 show the representative traces of the Ca^{2+} transient (A) and isometric tension (B) recorded from the preparations of the SLN-TG and NTG hearts. Both the peak of the Ca^{2+} transient ($p < 0.01$) and the peak of tension ($p < 0.01$) were significantly decreased in the SLN-TG hearts ($n = 7$ for SLN-TG, $n = 10$ for NTG). The TP did not significantly change, whereas the DT was significantly prolonged in the SLN-TG hearts ($p < 0.01$). Both the TPT ($p < 0.05$) and RT ($p < 0.01$) were significantly prolonged in the SLN-TG hearts.

3.5. Effects of selective downregulation of the SERCA activity on the SR function in the saponin-treated preparations

We then estimated the SR function in the SLN-TG and NTG hearts using the saponin-skinned preparations. The amount of Ca^{2+} uptake was significantly attenuated in the early phase (less than 15 s) of exposure to the loading solution at pCa 6.2 in the SLN-TG hearts (Fig. 4A) ($n = 11$ for SLN-TG, $n = 12$ for NTG). At the fixed loading time of 15 s, the amount of Ca^{2+} uptake was significantly decreased between pCa 6.6 and pCa 6.2 in the SLN-TG hearts (Fig. 4B) ($n = 18$ for SLN-TG, $n = 16$ for NTG). We also estimated the maximal Ca^{2+} content in the SR and found no significant differences between the SLN-TG and NTG hearts (Fig. 4C) ($n = 29$ SLN-TG, $n = 28$ for NTG).

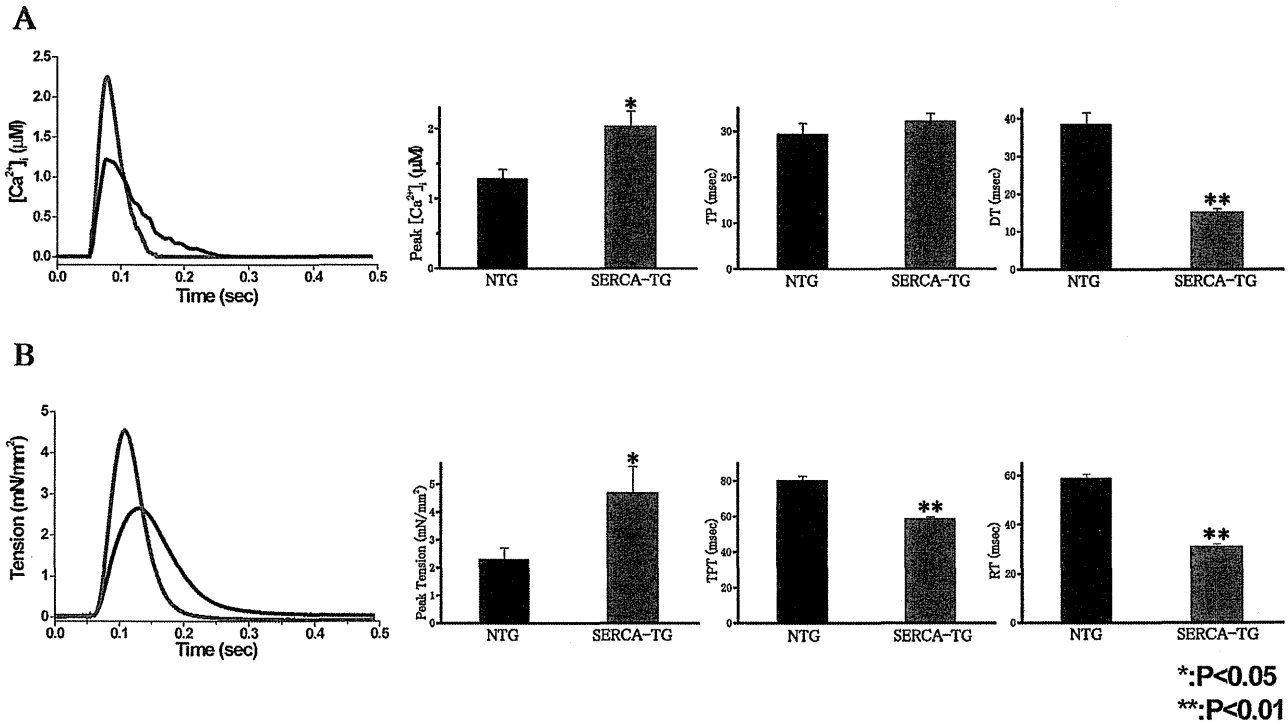

Fig. 1. Ca^{2+} transient and isometric tension in the intact preparations from the SERCA-TG hearts. (A) The left graph shows representative traces of the Ca^{2+} transient from the left ventricular papillary muscle in the SERCA-TG (red) and NTG (black) hearts. The bar graphs show the amplitude, time to reach the peak (TP) and decay time from the peak to half of the peak (DT) of the Ca^{2+} transient in the SERCA-TG (red) and NTG (black) hearts. (B) The left graph shows representative traces of isometric tension in the preparations obtained from the SERCA-TG (red) and NTG (black) hearts. The bar graphs show the amplitude, time to reach the peak (TPT) and relaxation time from the peak to half of the peak (DT) of tension in the SERCA-TG (red) and NTG (black) hearts.

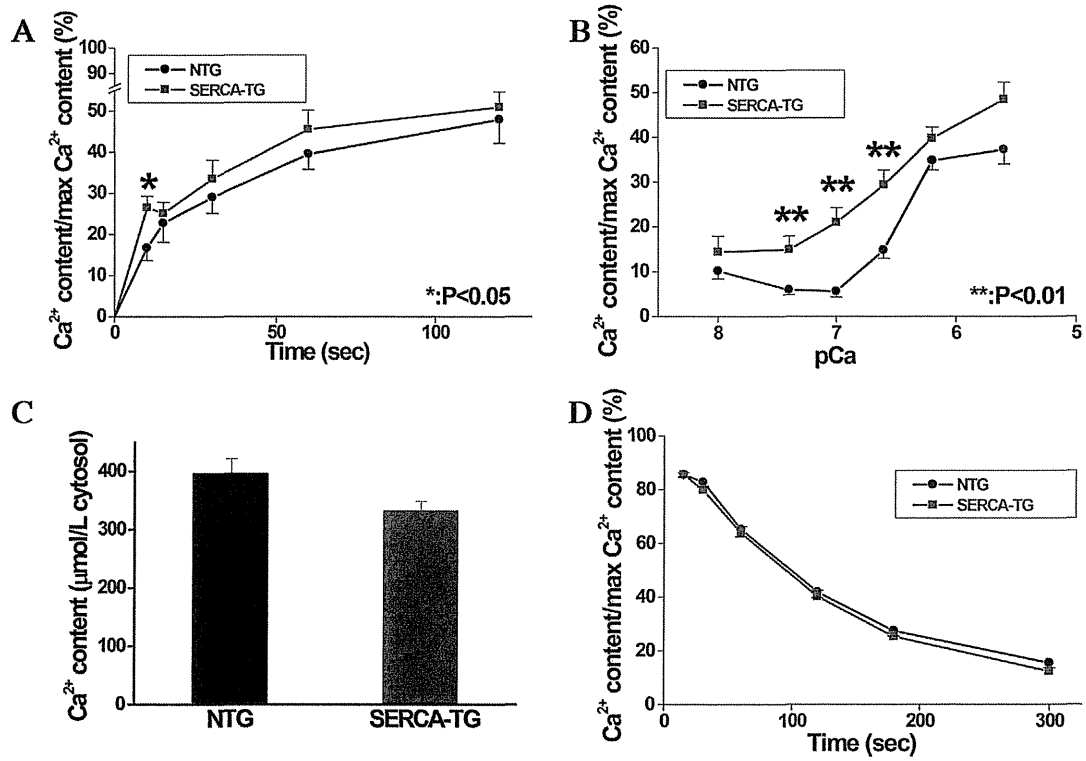

Fig. 2. Sarcoplasmic reticulum (SR) function in the saponin-treated preparations from the SERCA-TG hearts. (A) The time-dependent changes in Ca^{2+} uptake into the SR during exposure to the loading solution at pCa 7. (B) The Ca^{2+} uptake estimated at 10 s of exposure to the loading solution of various pCa. (C) The maximal Ca^{2+} content of the SR in the SERCA-TG and NTG hearts. (D) The time-dependent changes in Ca^{2+} leak from the SR following Ca^{2+} loading at pCa 6.2 for 120 s.

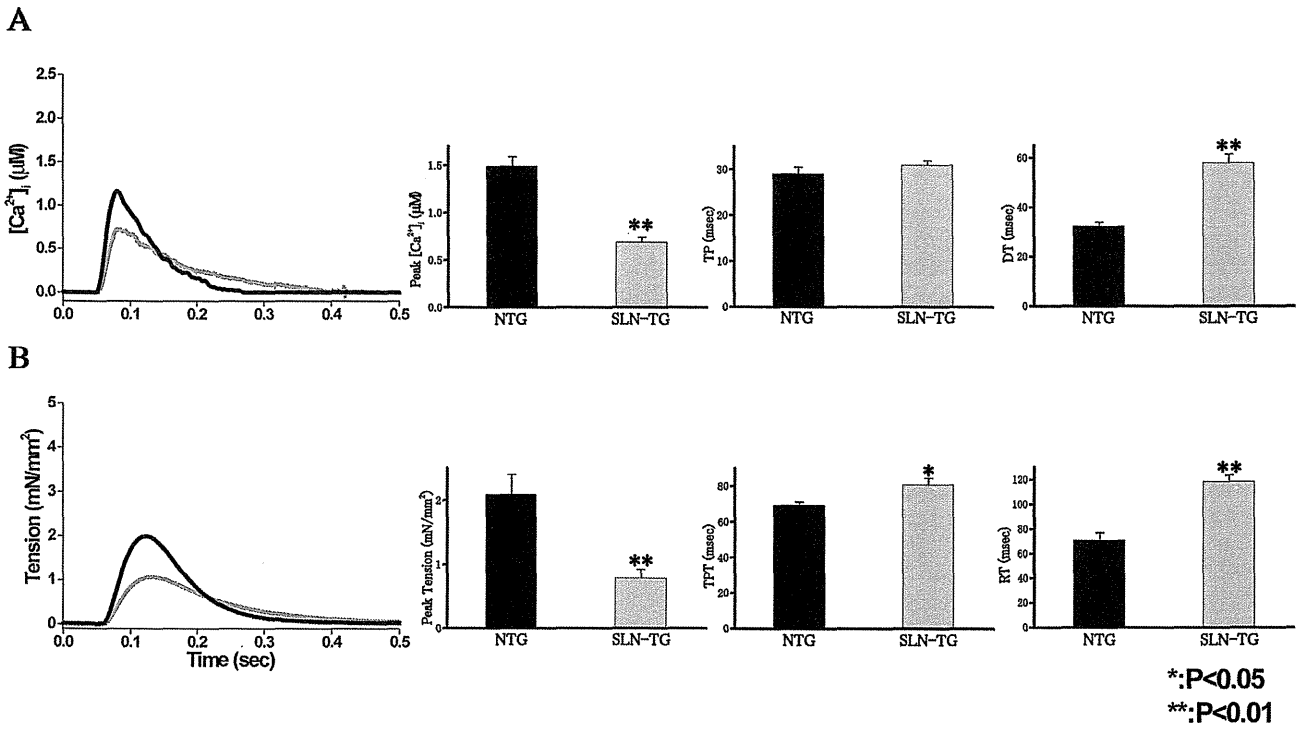

Fig. 3. Ca^{2+} transient and isometric tension in the intact preparations from the SLN-TG hearts. (A) The left graph shows representative traces of the Ca^{2+} transient from the left ventricular papillary muscle in the SLN-TG (green) and NTG (black) hearts. The bar graphs show the amplitude, time to reach the peak (TP) and decay time from the peak to half of the peak (DT) of the Ca^{2+} transient in the SLN-TG (green) and NTG (black) hearts. (B) The left graph shows representative traces of isometric tension in the preparations obtained from SLN-TG (green) and NTG (black) hearts. The bar graphs show the amplitude, time to reach the peak (TPT) and relaxation time from the peak to half of the peak (DT) of tension in the SLN-TG (green) and NTG (black) hearts.

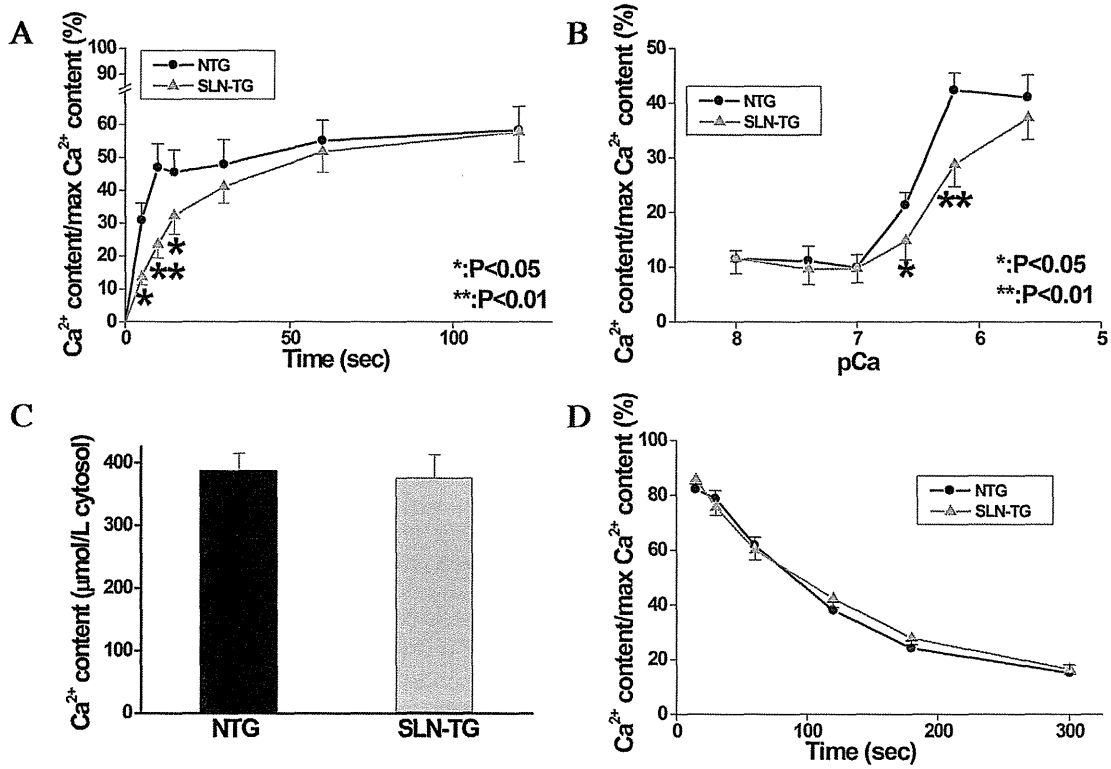

Fig. 4. Sarcoplasmic reticulum (SR) function in the saponin-treated preparations from the SLN-TG hearts. (A) The time-dependent changes in Ca^{2+} uptake into the SR during exposure to the loading solution at pCa 6.2. (B) The Ca^{2+} uptake estimated at 15 s of exposure to the loading solution of various pCa. (C) The maximal Ca^{2+} content of the SR in the SLN-TG and NTG hearts. (D) The time-dependent changes in Ca^{2+} leak from the SR following Ca^{2+} loading at pCa 6.2 for 120 s.